Article

Cell Stem Cell

Spatially Restricted Stromal Wnt Signaling Restrains Prostate Epithelial Progenitor Growth through Direct and Indirect Mechanisms

Graphical Abstract

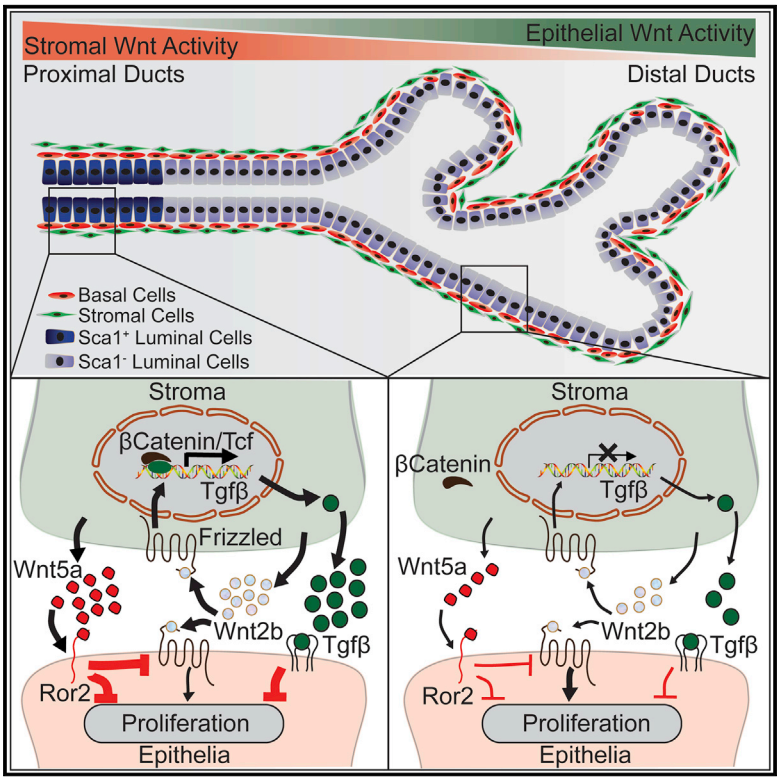

Highlights

- Stromal cells in mouse proximal prostatic ducts highly express multiple Wnt ligands
- Proximal duct stromal cells exhibit high Wnt/β-catenin activity
- Prostate stromal Wnt/β-catenin activity inhibits epithelial stem cell activity via TGFβ
- Spatially restricted stromal Wnt/β-catenin signaling is conserved across species

Authors

Xing Wei, Li Zhang, Zhicheng Zhou, ..., Chad J. Creighton, Michael M. Ittmann, Li Xin

Correspondence

xin18@uw.edu

In Brief

Wei et al. show that human and mouse prostate stromal cells exhibit region-specific differences in Wnt ligand expression and Wnt/β-catenin activity. Canonical and non-canonical Wnt signaling cooperate to restrain prostate stem or progenitor activity through direct and indirect TGFβ-dependent pathways.

Wei et al., 2019, Cell Stem Cell *24*, 753–768
May 2, 2019
https://doi.org/10.1016/j.stem.2019.03.010

CellPress

Cell Stem Cell
Article

Spatially Restricted Stromal Wnt Signaling Restrains Prostate Epithelial Progenitor Growth through Direct and Indirect Mechanisms

Xing Wei,[1,2,3] Li Zhang,[3] Zhicheng Zhou,[3] Oh-Joon Kwon,[3] Yiqun Zhang,[4] Hoang Nguyen,[1,5] Ruth Dumpit,[6] Lawrence True,[7] Peter Nelson,[6] Baijun Dong,[8] Wei Xue,[8] Walter Birchmeier,[9] Makoto M. Taketo,[10] Feng Xu,[11] Chad J. Creighton,[4,12] Michael M. Ittmann,[4,13,14] and Li Xin[1,3,15,16,*]

[1]Department of Molecular and Cellular Biology, Baylor College of Medicine, Houston, TX 77030, USA
[2]Graduate Program in Integrative Molecular and Biomedical Sciences, Baylor College of Medicine, Houston, TX 77030, USA
[3]Department of Urology, University of Washington, Seattle, WA 98109, USA
[4]Dan L. Duncan Comprehensive Cancer Center, Baylor College of Medicine, Houston, TX 77030, USA
[5]Center of Stem Cell and Regenerative Medicine, Baylor College of Medicine, Houston, TX 77030, USA
[6]Human Biology Division, Fred Hutch Cancer Research Center, Seattle, WA 98109, USA
[7]Department of Pathology, University of Washington, Seattle, WA 98109, USA
[8]Department of Urology, RenJi Hospital, School of Medicine, Shanghai Jiao Tong University, Shanghai, China
[9]Max Delbrück Center for Molecular Medicine (MDC), Robert-Rössle-Str. 10, 13092 Berlin, Germany
[10]Division of Experimental Therapeutics, Graduate School of Medicine, Kyoto University, Kyoto, Japan
[11]Institute of Molecular and Cell Biology, Agency for Science, Technology and Research, Singapore, Singapore
[12]Department of Medicine, Baylor College of Medicine, Houston, TX 77030, USA
[13]Department of Pathology and Immunology, Baylor College of Medicine, Houston, TX 77030, USA
[14]Michael E. DeBakey Department of Veterans Affairs Medical Center, Houston, TX 77030, USA
[15]Institute of Stem Cell and Regenerative Medicine, University of Washington, Seattle, WA 98109, USA
[16]Lead Contact
*Correspondence: xin18@uw.edu
https://doi.org/10.1016/j.stem.2019.03.010

SUMMARY

Cell-autonomous Wnt signaling has well-characterized functions in controlling stem cell activity, including in the prostate. While niche cells secrete Wnt ligands, the effects of Wnt signaling in niche cells per se are less understood. Here, we show that stromal cells in the proximal prostatic duct near the urethra, a mouse prostate stem cell niche, not only produce multiple Wnt ligands but also exhibit strong Wnt/β-catenin activity. The non-canonical Wnt ligand Wnt5a, secreted by proximal stromal cells, directly inhibits proliefration of prostate epithelial stem or progenitor cells whereas stromal cell-autonomous canonical Wnt/β-catenin signaling indirectly suppresses prostate stem or progenitor activity via the transforming growth factor β (TGFβ) pathway. Collectively, these pathways restrain the proliferative potential of epithelial cells in the proximal prostatic ducts. Human prostate likewise exhibits spatially restricted distribution of stromal Wnt/β-catenin activity, suggesting a conserved mechanism for tissue patterning. Thus, this study shows how distinct stromal signaling mechanisms within the prostate cooperate to regulate tissue homeostasis.

INTRODUCTION

Wnt signaling is a fundamental growth control pathway (Clevers et al., 2014; Nusse and Clevers, 2017). It has been shown to play critical roles in regulating stem cell self-renewal, pluripotency, proliferation, and regeneration in various organ systems (Korinek et al., 1998; Nguyen et al., 2009; Reya et al., 2003; Silva et al., 2008; van Amerongen et al., 2012). Wnt ligands are hydrophobic, tethered to cell membranes, and act as short-range morphogens (Nusse and Clevers, 2017). Therefore, Wnt signaling in stem cells is usually activated through the ligands produced by their adjacent niche cells, such as Paneth cells and telocytes in the small intestine (Sato et al., 2011; Shoshkes-Carmel et al., 2018), dermal papilla in the skin (Reddy et al., 2001), and stromal cells in the lung and mammary gland (Miller et al., 2012; Zhao et al., 2017), etc. However, much attention has been focused on understanding how stem cell-autonomous Wnt signaling affects its biology, whereas little is known regarding whether niche cells also possess active Wnt signaling and how this may affect the biology of the stem cells (Yamane et al., 2001). We seek to employ the prostate as an organ system to investigate how Wnt signaling in niche cells affects prostate stem cell biology.

Prostate epithelial cells turn over slowly, but they possess extensive regenerative potential when stimulated by cycles of androgen deprivation and replacement (Isaacs, 1985). There are three types of epithelial cells in the prostate: the predominant secretory luminal cells, the basal cells that sit between the luminal cells and basement membrane, and the rare neuroendocrine cells that are less well characterized. *In vivo* lineage tracing

studies have demonstrated that the basal and luminal cells in adult mice are independently sustained by their respective progenitors (Choi et al., 2012; Liu et al., 2011; Lu et al., 2013; Wang et al., 2013). Whether the human prostate epithelial lineage hierarchy is completely the same remains to be determined. However, the basal and luminal progenitors in humans and mice are both functionally plastic and exhibit facultative capability for at least bipotent differentiation under various experimental and pathological conditions (Chua et al., 2014; Collins et al., 2001; Goldstein et al., 2010; Karthaus et al., 2014; Kwon et al., 2014; Leong et al., 2008; Xin et al., 2005).

The mouse prostate surrounds the urethra at the base of the bladder. It contains 4 different lobes that consist of tubules budding outward away from the urethra. The tubular structures near the urethra are termed proximal prostatic ducts, whereas those at the tips are called distal ducts. The epithelial cells in the proximal ducts in adult mice, including both the basal and luminal cells, have been shown to retain bromodeoxyuridine (BrdU) or histone H_2B-GFP labeling and thereby are considered quiescent (Tsujimura et al., 2002; Zhang et al., 2018). We and others have shown that the stem cell activities of both the basal and luminal cell lineages are enriched in the proximal prostatic ducts (Burger et al., 2005; Kwon et al., 2016; Xin et al., 2005; Yoo et al., 2016).Therefore, the proximal prostatic duct has been considered a prostate stem cell niche in mice. However, how the signaling in this niche regulates prostate stem or progenitor activity is understudied.

Epithelial cell-autonomous Wnt/β-catenin signaling has been shown to regulate prostate stem cell specification, proliferation, and homeostasis. Wnt/β-catenin signaling is essential for prostate epithelial lineage specification during development (Francis et al., 2013; Lee et al., 2015; Simons et al., 2012) and for basal progenitors to generate luminal cells in adult mice (Lu and Chen, 2015). Although Wnt/β-catenin signaling is not necessary for the survival or proliferation of epithelial cells in adults (Francis et al., 2013; Simons et al., 2012), elevated epithelial Wnt/β-catenin signaling induces proliferation both *in vitro* and *in vivo* (Francis et al., 2013; Karthaus et al., 2014; Shahi et al., 2011; Simons et al., 2012; Yu et al., 2011). In contrast, little is known about whether active Wnt/β-catenin signaling is present in other cell lineages in the prostate stem cell niche and how it may affect prostate stem or progenitor activity. In this study, we show that Wnt/β-catenin signaling is active in the stromal cells at the prostate stem cell nice and demonstrate an important role of this stromal Wnt/β-catenin signaling in regulating prostate homeostasis.

RESULTS

Stromal Cells in Proximal Prostatic Ducts Express Wnt Ligands and Possess Active Wnt/β-Catenin Signaling

The mouse prostate stem cell activity is enriched at the proximal prostatic duct near the urethra, a prostate stem cell niche in mice (Figure S1A) (Burger et al., 2005; Kwon et al., 2016; Xin et al., 2005; Yoo et al., 2016; Zhang et al., 2018). Both basal and luminal cells in this region in adult mice are mitotically quiescent (Tsujimura et al., 2002). They express some lineage-specific antigens as expected (keratin 5/14 and P63 for basal cells; keratin 8 for luminal cells) (Figure S1B). However, the proximal luminal cells differ from distal luminal cells in that they express Sca-1 but not Nkx3.1 (Kwon et al., 2016) (Figure S1B). Using flow cytometric analyses, we found that even at the age of 5 weeks when the prostate is still undergoing active morphogenesis, BrdU was incorporated at a lower level in all three major cell lineages (basal, luminal, and stromal cells) at the proximal ducts than at the distal ducts (Figure 1). This result indicates that the lower proliferative potential is a persistent property of the proximal cells and led us to hypothesize that a unique signaling in the microenvironment at the proximal prostatic ducts suppresses the proliferative potential of the stem or progenitor cells.

To identify such signaling, we performed an RNA sequencing (RNA-seq) analysis using fluorescence-activated cell sorting (FACS)-isolated $Lin^-CD24^-CD49f^-Sca\text{-}1^+$ stromal cells from adult mouse proximal and distal prostatic ducts. Figure 2A shows that only 506 genes are differentially expressed by at least 1.4-fold. Interestingly, among the 309 genes that are upregulated in the proximal stromal cells, six are the core components of the Wnt signaling (*Wnt5a*, *Lgr5*, *Sfrp2*, *Sfrp3*, *Sfrp4*, and *Sfrp5*), which is further confirmed by qRT-PCR analysis (Figure 2B). Some *Sfrp*s were positively regulated by the Wnt/β-catenin signaling (Lescher et al., 1998). This prompted us to investigate whether the stromal cells possess active Wnt/β-catenin signaling. We performed a Wnt pathway-focused PCR array to compare the expression of 84 Wnt-related genes in FACS-sorted $Lin^-CD24^-CD49f^-Sca\text{-}1^+$ stromal cells from proximal and distal prostatic ducts. Figure 2C shows that 46 genes are significantly upregulated in the proximal stromal cells, including *Porcn*, an essential enzyme for Wnt ligand secretion, 10 Wnt ligands (*Wnt2*, *Wnt2b*, *Wnt3*, *Wnt4*, *Wnt5a*, *Wnt5b*, *Wnt6*, *Wnt8a*, *Wnt9a*, and *Wnt10a*), 9 receptor complex components (*Fzd2*, *Fzd3*, *Fzd4*, *Fzd5*, *Fzd6*, *Fzd7*, *Fzd8*, *Fzd9*, *Dvl2*, and *Lrp6*) and 9 typical Wnt downstream target genes (*Axin2*, *Sfrp2*, and *Lgr5*, etc.). The differential expression of several major genes is shown in Figure 2D and Table S1. The expression levels of these Wnt signaling components are much lower in the basal cells (Table S1). This result indicates that the proximal stromal cells not only produce Wnt ligands but also possess active Wnt/β-catenin signaling.

We performed RNA-*in situ* analyses to corroborate the spatially restricted expression patterns of three representative genes: *Wnt2b*, *Wnt5a*, and *Axin2*. Figure 2E shows that they are all highly expressed in the proximal stromal cells than in distal stromal cells. Interestingly, *Axin2* is expressed at a higher level in the distal epithelial cells than proximal epithelial cells, indicating a distinct spatially restricted pattern for the Wnt/β-catenin activity in both the epithelial and stromal cells.

Finally, we used a *TCF/LEF:H_2B-GFP* Wnt activity reporter mouse line to corroborate active Wnt/β-catenin signaling in the proximal stromal cells. This transgenic model harbors a nuclear-localized GFP-expressing cassette driven by a promoter containing 7xTCF/LEF consensus-binding sites (Ferrer-Vaquer et al., 2010). We showed previously that only the luminal cells at proximal ducts, but not those at distal ducts, express Sca-1 (Kwon et al., 2016). Co-immunostaining of GFP with Sca-1 and cytokeratin5 (K5), respectively, shows that 12% of the cells in the inter-glandular areas at the proximal ducts express GFP (Figure 2F, yellow arrows), whereas only 5% is GFP^+ at the distal ducts. These GFP^+ cells are mostly fibroblasts because they

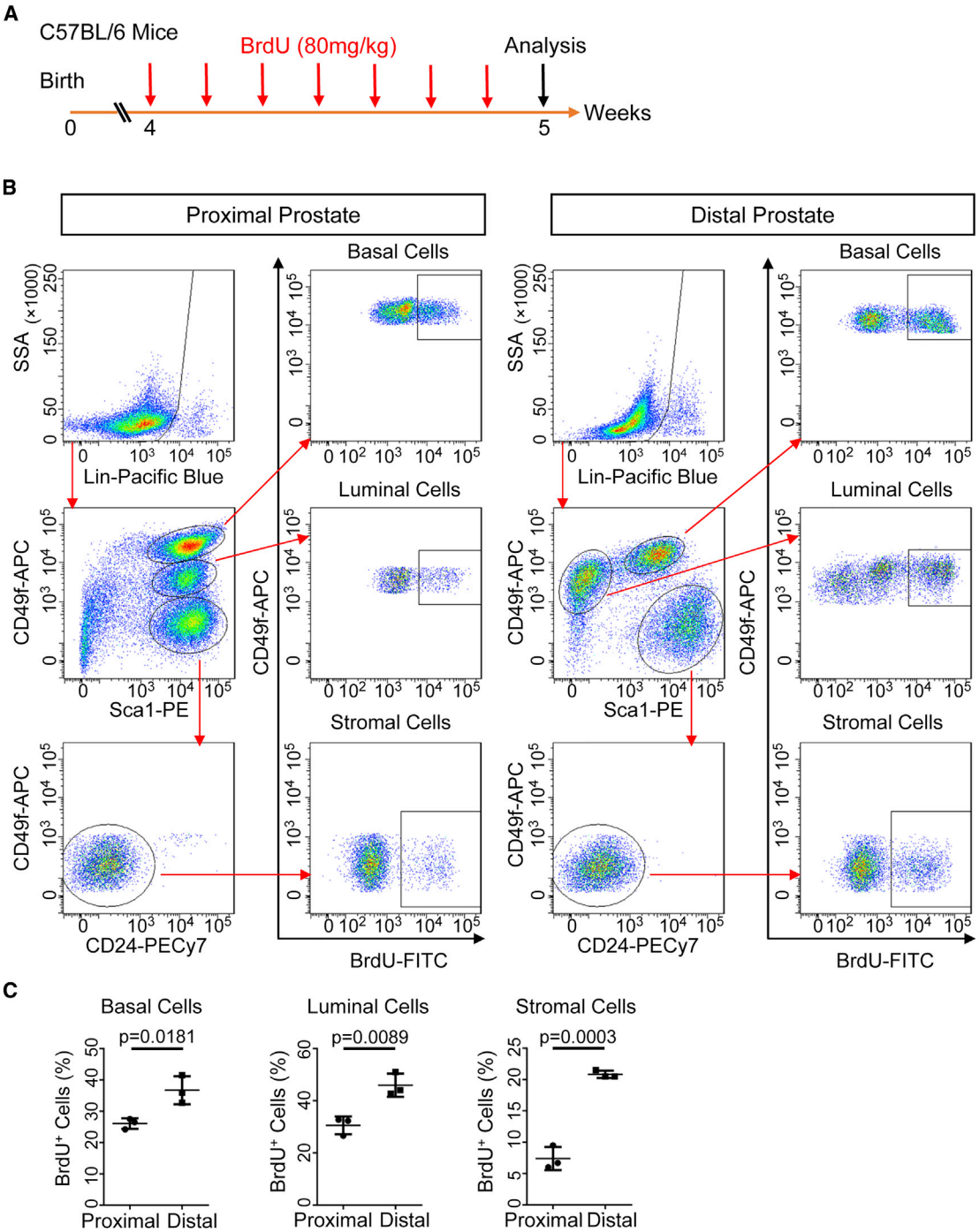

Figure 1. Mouse Proximal Prostate Cells Are Mitotically Quiescent Compared to Those at Distal Prostatic Ducts

(A) Schematic illustration of experimental design.

(B) FACS plots of BrdU$^+$ cells in Lin$^-$CD49f$^+$Sca-1$^+$ basal cells, Lin$^-$CD24$^-$CD49f$^-$Sca-1$^+$ stromal cells, Lin$^-$CD49f^{Low}Sca-1$^-$ distal luminal cells, and Lin$^-$CD49f^{Low}Sca-1$^+$ proximal luminal cells.

(C) Dot graphs show means ± SD of percentage of BrdU$^+$ cells in individual cell lineages from three independent experiments.

See also Figure S1.

express vimentin and very little α-smooth muscle actin, but not the markers for leukocytes (CD45) and endothelial cells (CD31) (Figure S2A). Note that there are more GFP$^+$ Wnt active epithelial cells in distal ducts (Figure 2F, white arrows), which is consistent with the RNA-*in situ* result (Figure 2E) showing that *Axin2* is expressed at a higher level in the distal epithelial cells.

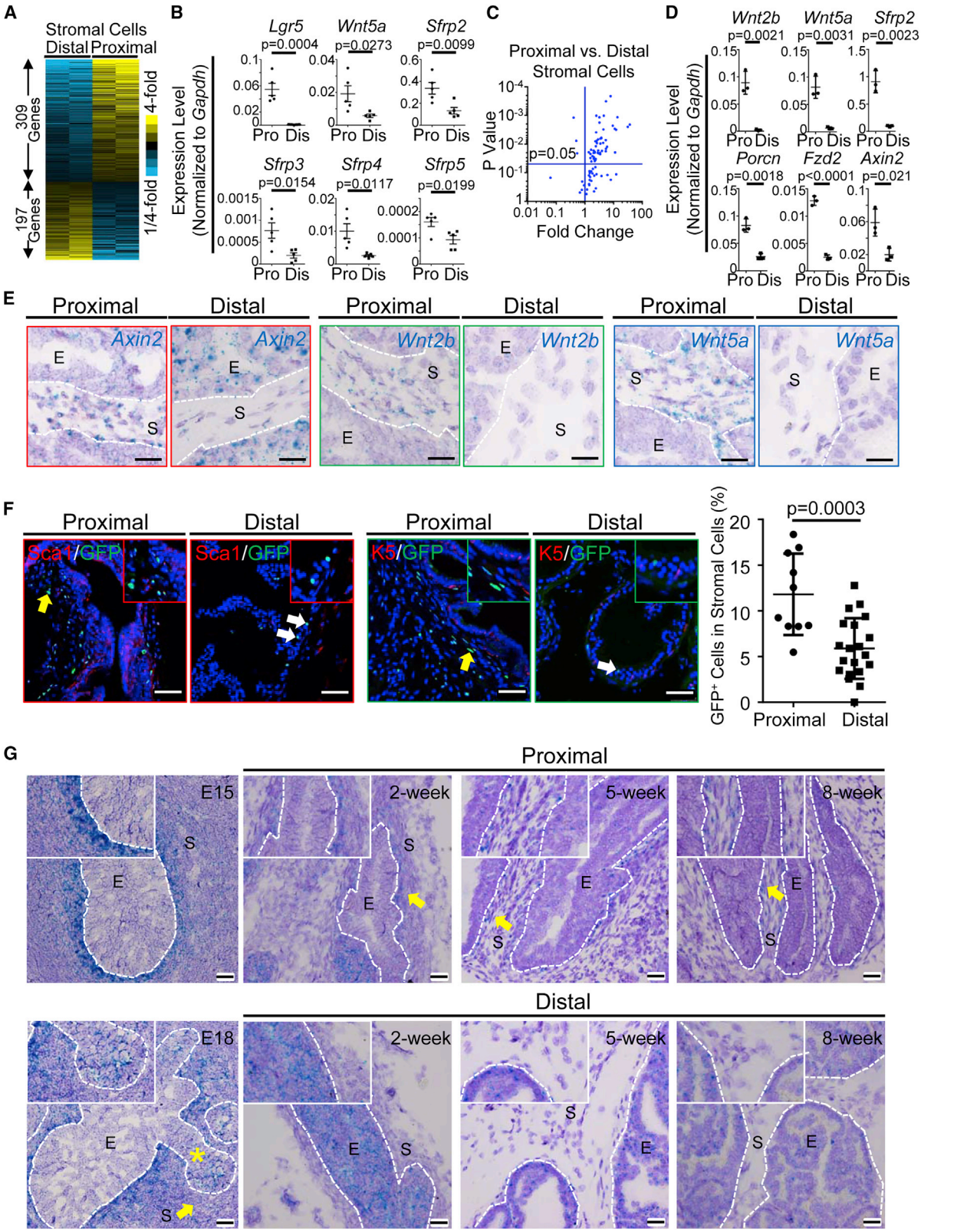

(legend on next page)

We further investigated the dynamics of *Axin2* expression during prostate development. Figure 2G shows that *Axin2* is strongly and almost exclusively expressed in the urogenital sinus mesenchyme cells (UGSM) at E15. By E18, UGS epithelia (UGSE) bud into the surrounding urogenital sinus mesenchyme cells. Interestingly, the expression of *Axin2* is lower in the mesenchyme surrounding the epithelial buds (Figure 2G, yellow arrows in E18 panel). By 2 weeks of age, it is already clear that *Axin2* is expressed at a higher level in the stromal cells at the proximal ducts than distal ducts, and this pattern remains the same at the 5 weeks and 8 weeks of age (Figure 2G, yellow arrows). On the other hand, *Axin2* is not expressed in UGSE at E15, but starts to be expressed at E18 in the epithelial cells especially those at the tips of epithelial buds (Figure 2G, asterisk in E18 panel). In 2-week-old mice, *Axin2* is predominantly expressed in the distal epithelial cells, but the expression declines at 5 and 8 weeks of age. The active stromal Wnt/β-catenin signaling during prostate development is also corroborated using the *TCF/LEF:H$_2$B-GFP* Wnt activity reporter mice (Figure S2B). Collectively, these studies reveal that the proximal stromal cells not only highly express Wnt ligands but also possess stronger Wnt/β-catenin activity than the distal stromal cells.

Non-canonical Wnt Signaling Suppresses Epithelial Proliferation at Proximal Prostatic Ducts

Wnt/β-catenin signaling can promote prostate epithelial proliferation (Karthaus et al., 2014; Shahi et al., 2011). Paradoxically, although the cells in the proximal ducts are exposed in a microenvironment with abundant Wnt ligands, their proliferative potential is lower. Some Wnt ligands (Wnt5a and Wnt4) expressed by the proximal stromal cells mediate non-canonical Wnt signaling. Wnt5a can suppress prostatic epithelial budding during early development (Huang et al., 2009). In addition, non-canonical Wnt signaling can antagonize the canonical signaling (Sato et al., 2010). Therefore, we reasoned that the lower proliferative potential of epithelial cells in proximal region is partly due to the non-canonical Wnt signaling.

We first examined the expression of the non-canonical Wnt receptors (*Ror1*, *Ror2*, and *Ryk*) in epithelial cells by qRT-PCR. Among them, *Ror2* is not only the most highly expressed but also expressed at a higher level in the proximal ducts than in distal ducts (Figures 3A and S3A). We performed co-immunostaining of Ror2 with K5 and Nkx3.1, respectively. Nkx3.1 is expressed by the luminal cells at distal ducts but not in those at proximal ducts (Kwon et al., 2016). Figure 3B corroborates a higher expression of Ror2 in both the proximal basal and luminal cells. We reasoned that the higher Wnt5a level at the proximal ducts mediates a higher non-canonical activity in the basal cells. To test this hypothesis, we compared the gene expression profiles of FACS-isolated Lin$^-$CD49f$^+$Sca-1$^+$ basal cells in adult mouse proximal and distal prostatic ducts using RNA-seq analyses. We found 765 genes that are differentially expressed by at least 1.4-fold between the two groups (Figure 3C). Figure 3D shows that several gene ontology biology processes related to the non-canonical Wnt signaling are enriched in the proximal basal cell group, including calcium ion binding, Rho protein signaling transduction, intermediate filament organization, apical plasma membrane, and regulation of establishment of planar polarity. The differential expressions of several representative genes that have been associated with noncanonical Wnt signaling in these Gene Ontology groups including *Camk2*, *Cdc42*, *Rhoj*, *Plce1*, *Wnt7b* (Zheng et al., 2013), and *Tnfrsf11a* (Maeda et al., 2012) were confirmed by qRT-PCR analysis (Figure S3B). These results support an enriched non-canonical Wnt activity in the proximal epithelial cells.

We further investigated how Wnt5a affects the prostate stem or progenitor activity. A prostate sphere assay (Xin et al., 2007) and a prostate organoid assay (Karthaus et al., 2014) have been widely used to measure the prostate basal and luminal stem or progenitor cell activity, respectively. In these assays, prostate stem or progenitor cells can form clonogenic spheres or organoids in defined media. Figure 3E shows that Wnt5a does not affect the sphere-forming activity but reduces the sphere size by 15%. The luminal cells (Sca-1$^+$) in proximal ducts also express a higher level of Ror2 than those at distal ducts (Figure 3A). The luminal cells are separated from the Wnt5a-generating stromal cells by only a thin layer of basal cells, so Wnt5a may diffuse in short distance to reach luminal cells. In addition, the proximal basal cells also express Wnt5a more than distal basal cells, although the expression level is much lower than in stromal cells (Figure S3C). Therefore, we also investigated how Wnt5a affects organoid growth from the Sca-1$^+$ proximal luminal cells. Figure 3F shows that Wnt5a also reduced the organoid size by 14%, although the organoid-forming activity was not affected significantly (Figure 3F). The reduction of

Figure 2. Mouse Proximal Prostatic Stromal Cells Express Wnt Ligands and Possess Active Wnt/β-Catenin Signaling

(A) Heatmap of RNA-seq analysis of FACS-isolated stromal cells from adult mouse proximal and distal prostatic ducts.

(B) qRT-PCR analysis of 6 representative Wnt pathway-related genes in FACS-isolated proximal and distal prostate stromal cells. Data represent means ± SD from five independent experiments. Pro, proximal stromal cells; Dis, distal stromal cells.

(C) Volcano plot shows fold differences and p value of expression levels of 84 Wnt-related genes between proximal and distal prostatic stromal cells determined by a Wnt pathway-focused RT^2 PCR profiler array.

(D) qRT-PCR analysis of 6 representative Wnt pathway-related genes identified in RT^2 PCR profiler array in FACS-isolated proximal and distal prostate stromal cells. Data represent means ± SD from three independent experiments. Pro, proximal stromal cells; Dis, distal stromal cells.

(E) RNA-*in situ* staining of *Axin2*, *Wnt2b*, and *Wnt5a* in anterior prostate of 8-week-old C57BL/6 mice. E, epithelial cells; S, stromal cells. Scale bars, 20 μm.

(F) Co-immunostaining of GFP/Sca-1 and GFP/K5 in anterior prostate of 8-week-old *TCF/LEF:H$_2$B-GFP* mice. Yellow arrows denote GFP$^+$ cells at inter-glandular areas at proximal ducts. White arrows show GFP$^+$ epithelial cells at distal ducts. Scale bars, 50 μm. Dot graph shows means ± SD of percentage of GFP$^+$ cells in proximal and distal prostate stromal cells from 3 mice. Each dot represents result from one image.

(G) RNA-*in situ* analysis of *Axin2* in E15 and E18 UGS, and anterior prostate of 2-, 5-, and 8-week-old C57BL/6 mice. E, epithelia; S, stroma. Yellow arrows and asterisk point to *Axin2* expression in stroma and epithelia, respectively. Scale bars, 20 μm.

See also Figure S2 and Table S1.

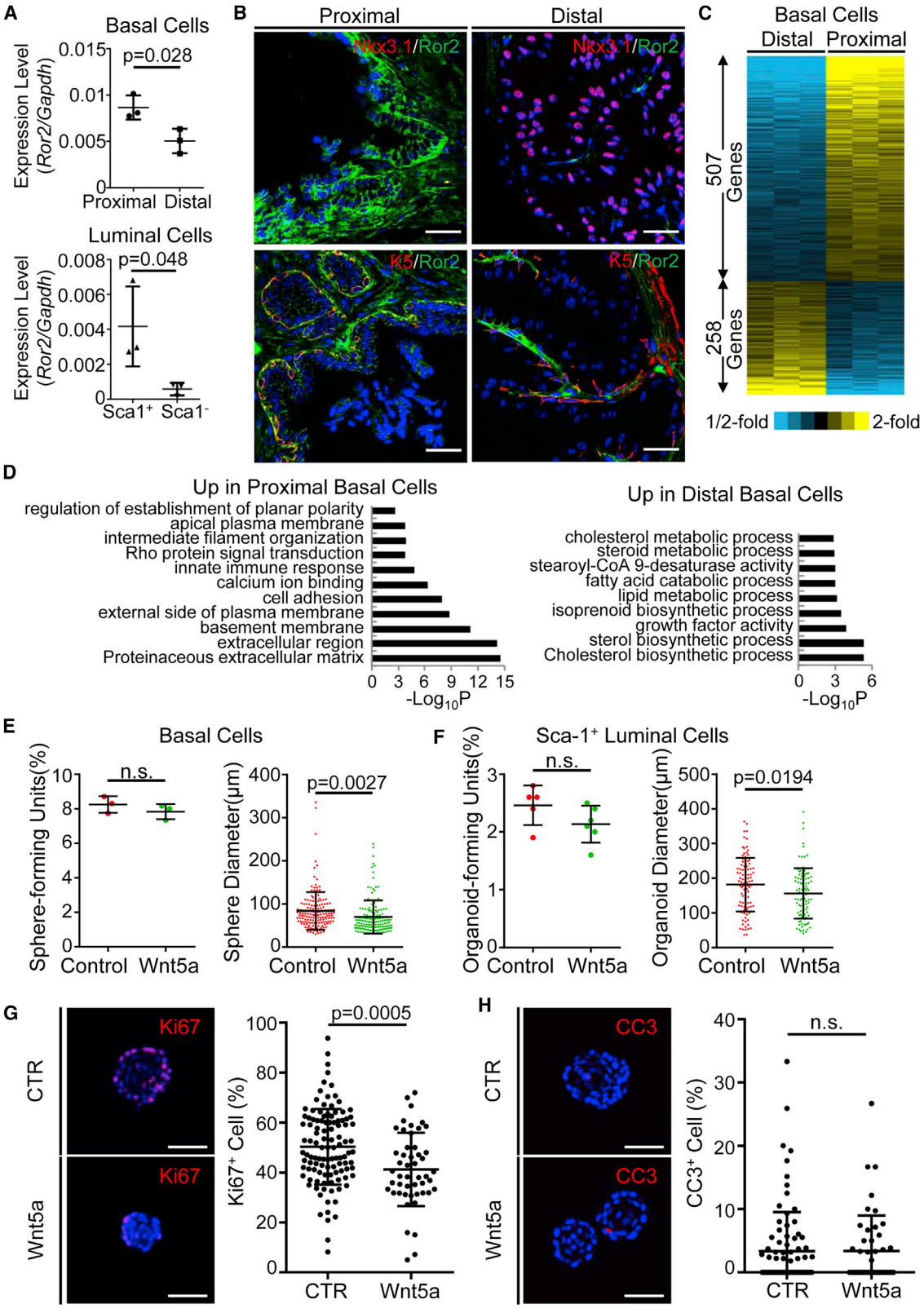

Figure 3. Non-canonical Wnt Signaling Suppresses Epithelial Proliferation at Proximal Ducts

(A) qRT-PCR of *Ror2* in FACS-isolated prostate basal and luminal cells at proximal and distal prostatic ducts. Data represent means ± SD from 3 independent experiments.

(legend continued on next page)

sphere size is due to decreased cell proliferation but not elevated apoptosis (Figures 3G and 3H).

The non-canonical Wnt signaling can antagonize the canonical Wnt signaling in other organ systems (Roarty et al., 2015; Sato et al., 2010). We confirmed that Wnt5a can suppress Wnt3a-stimulated *Axin2* expression in the prostate basal sphere cells (Figure S3D) and partially inhibit the Wnt3a-stimulated TCF/LEF reporter activity (Figure S3E). In addition, Wnt5a is less effective in reducing the size of prostate organoids in the absence of R-spondin (Figure S3F). These results support that the lower proliferative potential of the prostate stem or progenitor cells in the proximal ducts is partially caused through suppression of the Wnt/β-catenin signaling by Wnt5a.

Stromal Wnt/β-Catenin Signaling Suppresses Proliferation of Prostate Epithelial Cells

We next investigated how the stromal Wnt/β-catenin signaling affects the activity of prostate basal stem or progenitor cells. In the prostate sphere assay, embryonically derived urogenital sinus mesenchymal cells can stimulate sphere-forming activity of basal cells (Xin et al., 2007). We infected urogenital sinus mesenchyme cells with a control RFP-expressing lentivirus and a lentivirus expressing both RFP and a stabilized S37A β-catenin mutant separately (Figure S4A). Dissociated single mouse prostate epithelial cells were cocultured with the engineered urogenital sinus mesenchyme cells separately. Figure 4A shows that the sphere forming activity and size were reduced by 17% and 15%, respectively, in the S37A β-catenin group. Expression of a dominant-negative β-catenin in the S37A β-catenin-expressing urogenital sinus mesenchyme cells ablated their capacity to suppress prostate sphere growth and formation (Figure 4A). The S37A β-catenin-expressing and control stromal cells survived at the same rate in the assay, excluding the possibility that the reductions in sphere formation and size were caused by different stromal cell densities (Figure S4B). When the prostate spheres in the two groups were passaged with the control stromal cells separately, they formed secondary spheres of the same size and at the same frequency (Figure S4C). Collectively, these results suggest that the signaling mediated by the S37A β-catenin-expressing stromal cells suppress the proliferative potential of prostate sphere cells but not their capacity for self-renewal. The growth inhibitory effect of S37A β-catenin is not unique to urogenital sinus mesenchyme cells as we obtained the same results using primary adult mouse prostate stromal cells (Figure S4D).

We sought to corroborate the impact of the stromal Wnt signaling on prostate stem or progenitor cell activity *in vivo* using a prostate regeneration assay (Xin et al., 2003). Dissociated adult mouse prostate epithelial cells were mixed with the control and S37A β-catenin-expressing urogenital sinus mesenchyme cells separately and incubated under the renal capsules of immunodeficient male mice for 2 months. Figure 4B shows that the S37A β-catenin-expressing urogenital sinus mesenchyme cells are 50% less efficient than the control RFP-expressing urogenital sinus mesenchyme cells in promoting prostate regeneration. Immunostaining shows that there were 31% less $BrdU^+$ proliferating epithelial cells in the regenerated tissues in the S37A β-catenin group than in the control group (Figure 4C), whereas the apoptotic index was not different (Figure S4E). This study confirms that higher stromal Wnt/β-catenin signaling suppresses the proliferative potential of prostate stem or progenitor cells.

We further extended this study using genetically engineered mouse models. A *Col1a2-CreER*^{T2} model and a Ctnnb1$^{lox(ex3)}$ model (Harada et al., 1999) were used to genetically activate Wnt/β-catenin signaling in the prostate stromal cells. Using an eYFP reporter line, we demonstrated that the Col1a2-CreER^{T2} line can specifically and efficiently target prostate stromal cells (Figure S4F). Five-week-old Col1a2-CreER^{T2};Ctnnb1$^{lox(ex3)}$ bigenic mice were treated with tamoxifen to stabilize β-catenin in the prostate stromal cells (Figures S4G–S4I). Stabilization of β-catenin caused a reduction in prostatic weight and epithelial proliferative index (Figures S4J and S4K). However, stabilization of β-catenin in multiple organs through the Col1a2 promoter led to a 10% reduction in body weight, thickened skin, and smaller testis (Figure S4L), although the androgen receptor (AR) signaling is not altered as indicated by the strong epithelial AR nuclear staining (Figure S4M). To further corroborate that the reduced prostate size was a direct consequence of β-catenin activation in the prostate stromal cells, we transplanted anterior prostate tissues of 3-week-old Col1a2-CreER^{T2};Ctnnb1$^{lox(ex3)}$ and Col1a2-CreER^{T2} mice under the renal capsules of immunodeficient male hosts. The hosts were treated with tamoxifen to turn on the stromal expression of the stabilized β-catenin in the xenografts. The xenografts were collected 4 weeks later (Figure 4D). Figure 4E shows that the average weight of the xenografts in the Col1a2-CreER^{T2};Ctnnb1$^{lox(ex3)}$ group is only 85% of that in the control group. The proliferative index of epithelial cells in the Col1a2-CreER^{T2};Ctnnb1$^{lox(ex3)}$ group was 53% less than that of the control group (Figure 4F). Collectively, these results demonstrate that activation of Wnt/β-catenin signaling in the stromal cells suppresses prostate epithelial proliferation.

Conversely, we utilized the Col1a2-CreER^{T2} and Ctnnb1$^{loxp/loxp}$ models (Huelsken et al., 2001) to disrupt Wnt/β-catenin signaling in the prostate stromal cells (Figure 4G). qRT-PCR analyses confirmed that β-catenin was specifically and efficiently knocked out in ~70% of the prostate stromal cells (Figures S4N–S4P).

(B) Immunostaining of Ror2, Nkx3.1, and keratin 5 (K5) in anterior prostates of 8-week-old C57BL/6 mice. Scale bars, 50 μm.
(C) Heatmap of RNA-seq analysis of FACS-isolated basal cells from proximal and distal prostatic ducts.
(D) Gene ontology analysis of RNA-seq of FACS-isolated basal cells from proximal and distal prostatic ducts.
(E) Sphere-forming units and sphere sizes of FACS-isolated prostate basal cells with and without 100 ng/mL Wnt5a. Data show means ± SD from 3 independent experiments. Data of sphere size show results of one representative experiment unless otherwise noted.
(F) Organoid-forming units and organoid sizes of FACS-isolated prostate Sca-1^+ luminal cells with and without 100 ng/mL Wnt5a. Data show means ± SD from 5–6 independent experiments. n.s., not significant.
(G and H) Immunostaining of Ki67 (G) and Cleaved caspase 3 (CC3) (H) in spheres treated with Wnt5a and without Wnt5a (CTR). Each dot represents result from one sphere.
See also Figure S3.

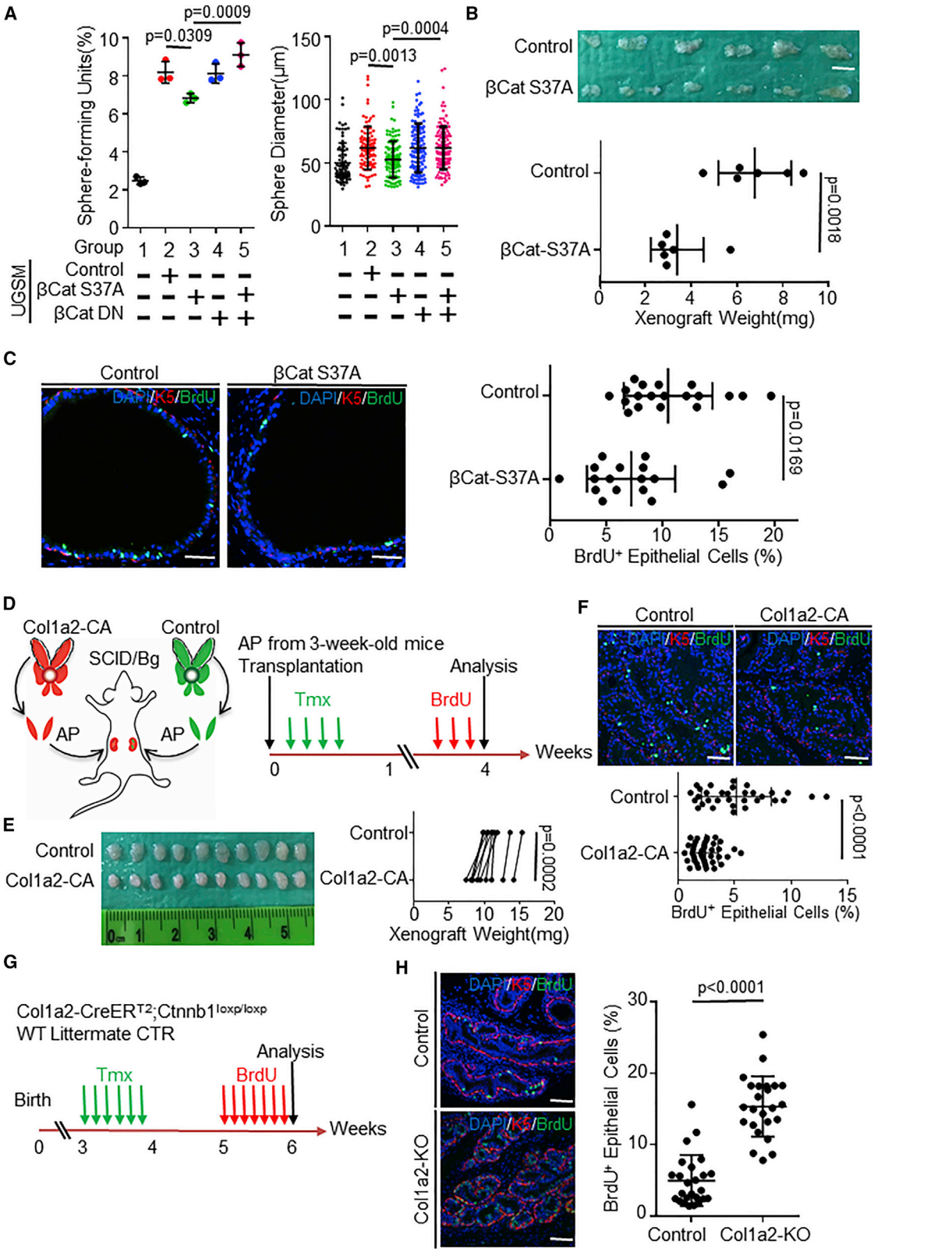

(legend on next page)

Immunostaining shows that the proliferative index of epithelial cells in the *Col1a2-CreER^{T2};Ctnnb1$^{loxp/loxp}$* mice was 3-fold higher than that in the control group (Figure 4H). Collectively, these results demonstrate that stromal Wnt/β-catenin activity suppresses prostate epithelial proliferation.

Wnt/β-Catenin Signaling Transcriptionally Upregulates Transforming Growth Factor β Ligands in Prostate Stromal Cells

Using a chamber assay, we demonstrated that direct contact between the stromal and basal cells is not necessary for the S37A β-catenin-expressing stromal cells to suppress prostate sphere formation and growth (Figures S5A–S5C). This indicates that the inhibitory effect is mediated via paracrine factors. To identify the factors, we compared the gene expression profiles of the primarily cultured adult mouse prostate stromal cells that express S37A β-catenin and the control cells that only express RFP. We identified 783 genes that were differentially expressed by at least 1.2-fold (Figure 5A). Figure 5B summarizes the differentially enriched Gene Ontology biological processes. As expected, genes associated with the Wnt receptor signaling pathway is enriched in the S37A β-catenin group. Of note, we did not observe upregulation of *Sfrps* by β-catenin (Figure S5D), suggesting that the higher expression of *Sfrp*s in the proximal stromal cells may not reflect a negative feedback of the Wnt/β-catenin signaling.

Platelet-derived growth factor (PDGF) receptor and transforming growth factor β (TGFβ) receptor binding are the other two Gene Ontology entries enriched in the S37A β-catenin group. Although *Pdgfc* is upregulated in the S37A β-catenin group, blocking its activity did not alleviate the growth inhibitory effect of the S37A β-catenin-expressing stromal cells on the prostate spheres (Figures S5E and S5F). We therefore focused on the TGFβ signaling. qRT-PCR analysis confirms that *Tgfβ2* and *Tgfβ3* were upregulated by 2.3- and 1.4-fold, respectively, in the S37A β-catenin-expressing prostate stromal cells, but the expression of *Tgfβ1* was not significantly different (Figure 5C). These observations suggest that *Tgfβ2* and *Tgfβ3* may be upregulated by Wnt signaling in the prostate stromal cells. Consistently, both ligands were downregulated in the FACS-isolated prostate stromal cells from tamoxifen-treated *Col1a2-CreER^{T2};Ctnnb1$^{loxP/loxP}$* mice than in those of the control *Col1a2-CreER^{T2}* mice, although the reduction of *Tgfβ3* was not statistically significant (Figure 5D). Conversely, in the FACS-isolated stromal cells from proximal prostatic ducts where Wnt signaling is higher, *Tgfβ2* is expressed at 3.5-fold higher than in those from distal ducts (Figure 5E).

We investigated how Wnt signaling upregulates *Tgfβ2* and *Tgfβ3*. There are 2 TCF/LEFs consensus binding sites [(A/T)(A/T)CAAAG] (Yochum et al., 2008) in a 2-kb fragment upstream of the translational start codon (TSC) of *Tgfβ2*, whereas 5 sites are presented 4 kb upstream of TSC of *Tgfβ3* (Figure 5F). We cloned these 2 fragments into the pGL3 luciferase reporter and transfected them into primarily cultured mouse prostate stromal cells. Figure 5G shows that S37A β-catenin increased the luciferase activity by 1.9- and 1.7-fold, respectively, whereas the induction of the luciferase activity was abolished when these TCF/LEFs consensus binding sites were deleted or mutated. Chromatin immunoprecipitation analysis demonstrated that β-catenin directly binds to two of these sites in primary mouse prostate stromal cells (Figure 5H). Collectively, these results show that β-catenin transcriptionally activates *Tgfβ2* and *Tgfβ3* in the prostate stromal cells.

Wnt/β-Catenin-Active Prostate Stromal Cells Suppress Basal Cell Proliferation via TGFβ

Because Tgfβ suppresses prostate basal stem or progenitor activity (Valdez et al., 2012), we reasoned that stromal Wnt/β-catenin signaling suppresses basal stem cell proliferation via Tgfβ. To test this hypothesis, we introduced a dominant-negative TgfβRII (dnTgfβRII) into the prostate basal stem cells to disrupt their capability to respond to all the Tgfβs (Figure S6A). Briefly, FACS-isolated basal stem cells were infected with a lentivirus that expresses both dnTgfβRII and GFP and a control GFP lentivirus, separately. Infected basal cells were cocultured with the control and S37A β-catenin-expressing primary prostate stromal cells separately in the sphere assay. Consistent with the result shown in Figure 4A, compared to the RFP-expressing stromal cells, the S37A β-catenin-expressing stromal cells suppressed the sphere formation and growth of prostate basal cells (Figures 6A and 6B, groups 2 versus 3). In contrast, the sphere forming activity and size were not significantly different when dnTgfβRII-expressing basal cells were cocultured with the

Figure 4. Stromal Wnt/β-Catenin Signaling Suppresses Proliferation of Prostate Basal Stem Cell

(A) Sphere-forming units and sphere sizes of prostate epithelial cells cultured without urogenital sinus mesenchyme (UGSM) cells, with control wild-type UGSM cells, with UGSM cells expressing S37A-βcatenin, and with UGSM cells expressing dominant-negative (DN) βcatenin, respectively. Data show means ± SD from 3 independent experiments.

(B) Transillumination image of regenerated prostate tissues. Scale bar, 5 mm. Dot graph shows means ± SD of weight of xenografts. n = 6.

(C) Co-immunostaining of BrdU and K5 in regenerated prostatic tissues derived from prostate epithelial cells stimulated by control urogenital sinus mesenchyme cells and urogenital sinus mesenchyme cells expressing S37A-βcatenin. Scale bars, 50 μm. Dot graph shows means ± SD of percentage of BrdU$^+$ epithelial cells in regenerated prostatic tissues. Each dot represents result from one image. Data collected from 4 pairs of independent samples.

(D) Schematic illustration of experimental design. Control, wild type (WT) littermate mice; Col1a2-CA, Col1a2-CreERT2;Ctnnb1$^{lox(ex3)}$ mice; Tmx, tamoxifen; AP, anterior prostate.

(E) Transillumination images of prostatic xenografts after tamoxifen treatment. Dot graph shows quantification of weight of 10 pairs of xenografts analyzed by paired t test.

(F) Co-immunostaining of BrdU and K5 in prostatic xenografts. Scale bars, 50 μm. Dot graph shows means ± SD of percentage of BrdU$^+$ epithelial cells in prostatic xenografts. Each dot represents result from one image.

(G) Schematic illustration of experimental design. Tmx, tamoxifen.

(H) Co-immunostaining of BrdU and K5 in anterior prostates of Col1a2-CreERT2;Ctnnb1$^{loxp/loxp}$ (Col1a2-KO) and littermate C57BL/6 (control) mice. Scale bars, 50 μm. Dot graph shows means ± SD of percentage of BrdU$^+$ epithelial cells. Each dot represents result from one image. Data collected from 4 pairs of mice. See also Figure S4.

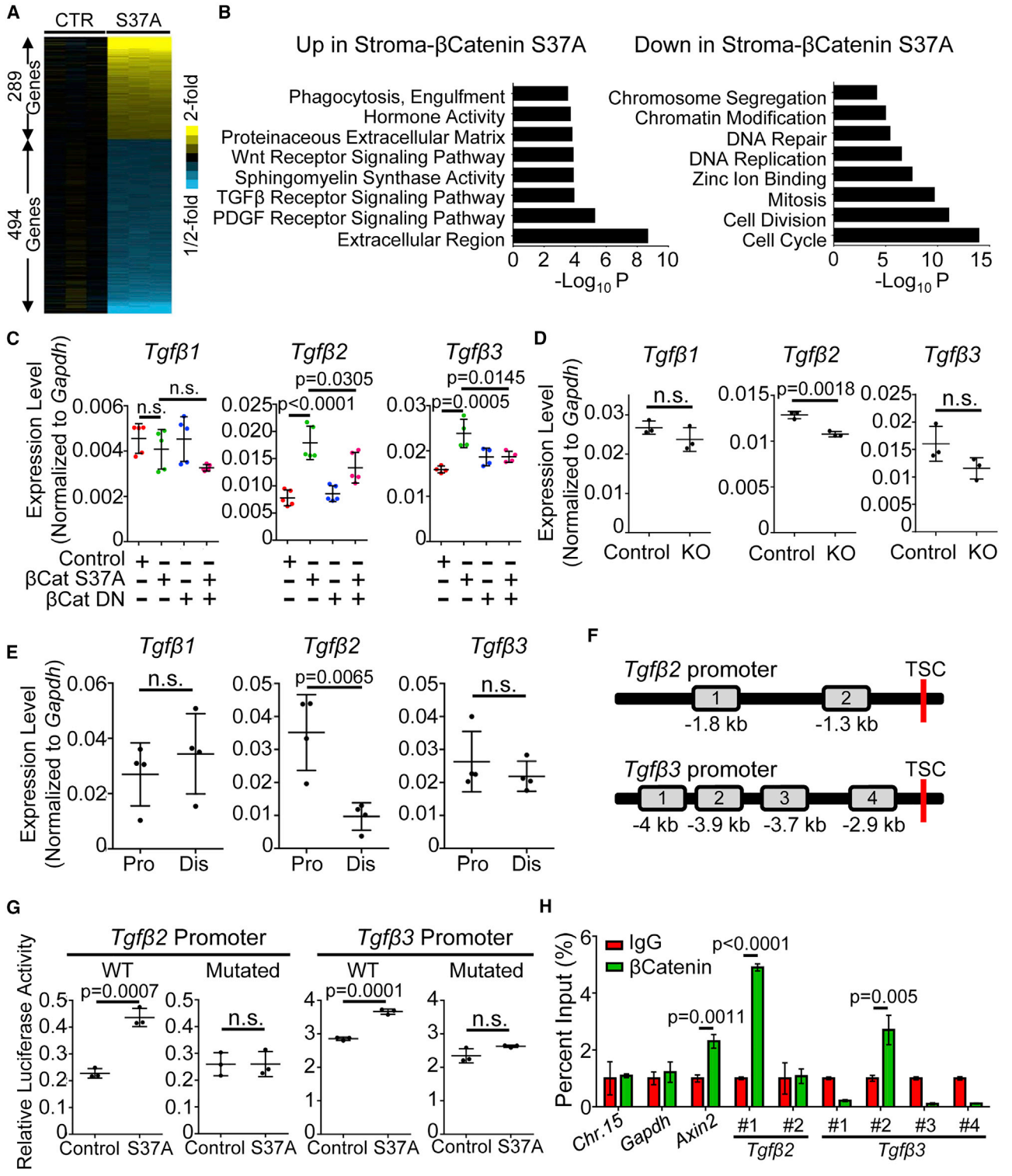

Figure 5. β-Catenin Transcriptionally Upregulates Tgfβ Ligands in Prostate Stromal Cells

(A) Heatmap of RNA-seq analysis of control and β-catenin S37A-expressing primary prostate stromal cells. The heatmap depicts fold changes in experiment versus control. Each gene is centered on average of control.

(B) Gene ontology analysis of RNA-seq analysis of control and β-catenin S37A-expressing prostate stromal cells.

(C) qRT-PCR analysis of *Tgfβ1*, *Tgfβ2*, and *Tgfβ3* in urogenital sinus mesenchyme cells that express red fluorescent protein only (control), β-catenin S37A, and dominant-negative (DN) β-catenin. Dot graphs represent means ± SD from 5 independent samples.

(legend continued on next page)

S37A β-catenin-expressing and RFP-expressing stromal cells, respectively (Figures 6A and 6B, groups 5 versus 6). Because not all basal cells were infected by the dnTgfβRII-GFP lentivirus, only ~70% of the prostate spheres in this group expressed GFP. The mean size of the GFP^+ spheres derived from dnTgfβRII-expressing basal cells was 1.3-fold larger than that of the GFP^- spheres derived from the uninfected basal cells (Figure 6B, groups 6 versus 6a). This further demonstrates that disrupting Tgfβ signaling desensitizes basal cells from the growth inhibitory effect of stromal Wnt/β-catenin signaling. Similarly, when a Pan-Tgfβ blocking antibody was added in the sphere assay to neutralize the activity of Tgfβs, the growth inhibitory effect of the S37A β-catenin-expressing stromal cells on prostate spheres was ablated (Figure S6B). This further corroborates that Tgfβ plays a critical role in the growth inhibition of prostate spheres mediated by the stromal Wnt/β-catenin signaling.

Finally, we employed the prostate regeneration assay to corroborate the finding *in vivo*. The control and dnTgfβRII-expressing prostate epithelial cells were incubated with S37A β-catenin-expressing urogenital sinus mesenchyme cells separately under the renal capsules of immunodeficient male mice for 2 months. Figure 6C shows that the mean weight of regenerated tissue in the dnTgfβRII group is 2-fold heavier and these tissues contain more regenerated glands (Figure S6C). The proliferative index of epithelial cells was 1.8-fold higher in the dnTgfβRII group (Figure 6D). Collectively, these studies demonstrate that Tgfβ plays a critical role in the growth inhibitory effect mediated by the Wnt active prostate stromal cells.

Wnt/β-Catenin Signaling Is Higher in Stromal Cells of Human Transition Zone than in Peripheral Zone Prostate

Anatomically, the mouse and human prostate glands are different. The human prostate is defined into 4 different zones, of which the peripheral zone (PZ) and transition zone (TZ) are the two major zones (McNeal et al., 1988). PZ covers the dorsolateral and apical parts of the gland, whereas TZ is located between the proximal prostatic urethra and lateral parts of the PZ. Despite the anatomic difference, the mouse proximal prostatic ducts and human TZ share some similarities. They are both anatomically closer to the urethra compared to other prostatic regions. In addition, epithelial cells in mouse proximal prostatic ducts and human TZ are both mitotically inert compared to those in mouse distal ducts and human PZ, respectively (Colombel et al., 1998; Tsujimura et al., 2002). Based on these similarities, we hypothesized that the stromal cells in human TZ also possess higher Wnt/β-catenin signaling than those in PZ.

We obtained 9 pairs of TZ and PZ stromal cells from formalin-fixed paraffin-embedded normal human TZ and PZ tissues by laser capture microdissection (Figure S7A) and performed a qRT-PCR analysis of *AXIN2*, *WNT5A*, *TGFB1*, *TGFB2*, and *TGFB3*. Figure 7A shows that all these genes except *TGFB1* are expressed at a higher level in the TZ stromal cells than in the PZ stromal cells. We attempted to confirm the results using an RNA-*in situ* analysis. The probes for *WNT5A* and *TGFB2* stained too weak in human specimens to be quantitated convincingly. Figure 7B shows representative staining of *AXIN2* in TZ and PZ of the same donor. In TZ, *AXIN2* staining is mostly observed in the stromal cells that are immediately adjacent to epithelial glandular structures. In comparison, staining in the stromal cells adjacent to epithelial glands in PZ is weaker. Quantification of pairwise comparison shown in Figure 7C demonstrates that the difference is statistically significant. Interestingly, expression of *AXIN2* appears higher in epithelial cells in PZ than in TZ (Figure S7B). The anatomically distinct expression patterns of *AXIN2* between epithelial cells in TZ and PZ are very similar to those observed between mouse proximal and distal prostatic ducts (Figure 2E). Similarly, the expression of *TGFB3* in stromal cells of TZ is also significantly higher than that in stromal cells in PZ (Figures 7D and 7E). These results support that the differential expression of these genes in distinct anatomic locations is a conserved mechanism for tissue morphogenesis across different species.

DISCUSSION

Heterogeneity of tissue-resident stromal cells has been widely appreciated. Our study reveals that the stromal cells in different anatomic prostatic regions express different levels of Wnt ligands and exhibit distinct levels of Wnt/β-catenin activity, which influence prostate epithelial stem or progenitor cell activity, directly and indirectly. It should be noted that these two mechanisms may not be totally independent because TGFβ can regulate expression of both canonical and noncanonical Wnt ligands (Placencio et al., 2008; Roarty and Serra, 2007). The two mechanisms are also not exclusive as Wnt2 was shown to regulate prostate growth probably by downregulating FGF10 in stroma (Madueke et al., 2018). Our study in the prostate provides another example of the phenotypic and functional heterogeneity of the tissue resident stromal cells and raises more questions. For example, how do the Wnt/β-catenin active stromal cells turn over, and do they possess mesenchymal stem cell potential? Future studies using

(D) qRT-PCR analysis of *Tgfβ1*, *Tgfβ2*, and *Tgfβ3* in FACS-isolated stromal cells from Tmx-treated Col1a2-$CreER^{T2}$;$Ctnnb1^{loxp/loxp}$ (KO) and WT littermate control mice. Dot graphs represent means ± SD from 3 pairs of mice.

(E) qRT-PCR analysis of *Tgfβ1*, *Tgfβ2*, and *Tgfβ3* in FACS-isolated stromal cells from proximal and distal prostatic ducts. Dot graphs represent means ± SD from 4 pairs of mice.

(F) Schematic illustration of loci of TCF/LEF binding sites at promoters of *Tgfβ2* and *Tgfβ3*. Two adjacent TCF/LEF binding sites at −4 kb of *Tgfβ3* promoter are represented in box 1. TSC, translational start codon.

(G) Luciferase reporter assays determine activity of *Tgfβ2* and *Tgfβ3* luciferase reporters in prostate stromal cells expressing red fluorescent protein only (control) and S37A β-catenin. Dot graphs represent means ± SD from 3 experiments.

(H) Chromatin immunoprecipitation analysis of binding of anti-β-catenin antibody and IgG control to promoters of *Tgfβ2* and *Tgfβ3* in β-catenin S37A-expressing prostate stromal cells. Two sites at Chr.15 and *Gapdh* are used as controls for no binding, whereas a site at *Axin2* is used as positive control for binding. Histograms show means ± SD of relative enrichment from 3 independent experiments.

See also Figure S5.

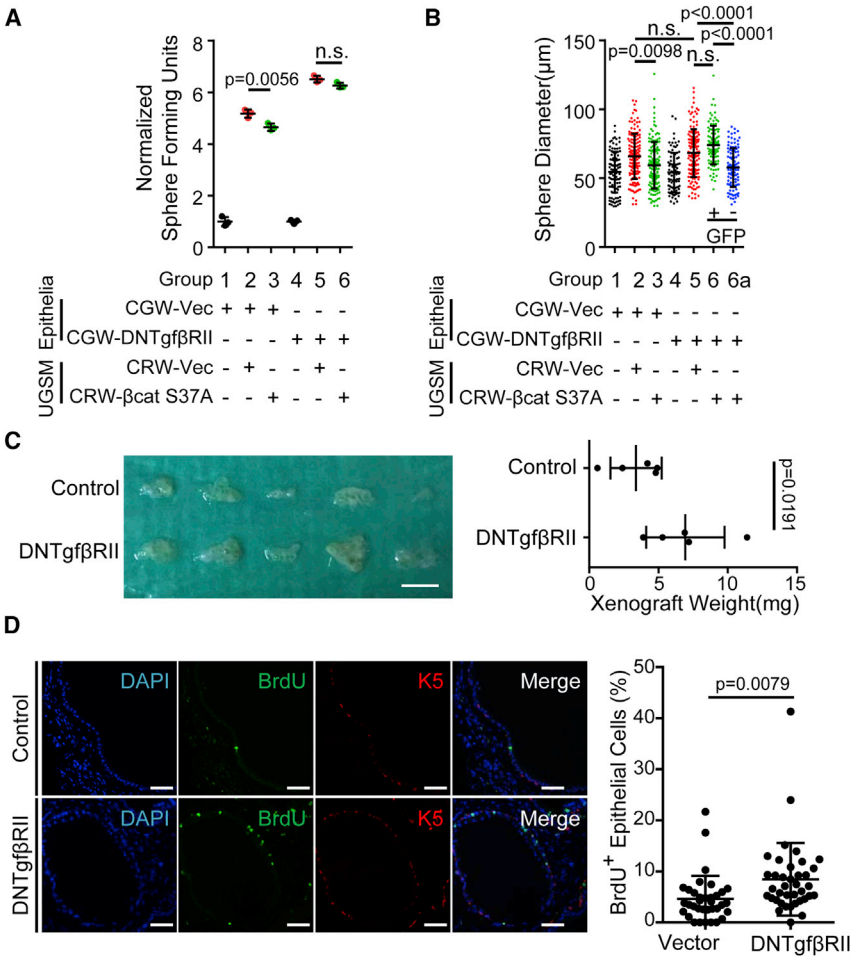

Figure 6. Wnt/β-Catenin-Active Prostate Stromal Cells Suppress Basal Cell Proliferation via *Tgfβ*

(A and B) Dot graphs quantify sphere-forming units (A) and sphere sizes (B) derived from prostate epithelial cells co-cultured with and without urogenital sinus mesenchyme cells. Epithelial cells are infected by lentivirus expressing GFP (CGW-control) or dominant-negative (DN) TgfβRII, whereas urogenital sinus mesenchyme cells are infected by lentivirus that express RFP (CRW-control) or S37A β-catenin. Data show means ± SD from three independent experiments. n.s., not significant.

(C) Transillumination images of regenerated prostate tissues derived from prostate epithelial cells infected with lentivirus expressing GFP (control) and dominant-negative (DN) TgfβRII, respectively. Scale bar, 5 mm. Dot graph shows means ± SD of xenograft weight. n = 5.

(D) Co-immunostaining of BrdU and K5 in regenerated prostatic tissues. Scale bars, 50 μm. Dot graph shows means ± SD of percentage of $BrdU^+$ epithelial cells in regenerated prostatic tissues. Each dot represents result from one image. Data were collected from 4 pairs of regenerated prostatic tissues.

See also Figure S6.

the single-cell analysis and lineage tracing approach should address their features in more detail.

Molecular Mechanisms that Regulate Expression of Wnt ligands and Activation of Wnt Signaling

We showed that Wnt ligands are predominantly expressed in the stromal cells in the mouse prostate. In addition, the expression levels of the Wnt ligands such as *Wnt2* and *Wnt5a* are higher in the proximal stromal cells. The molecular mechanisms underlying this differential expression pattern remains unclear. Previous studies have shown that Wnt ligands can be regulated by various mechanisms. First, growth factors and transcription factors such as Fgf, Hgf, Hox5, and Gli proteins can regulate expression of *Wnt* ligands (Hrycaj et al., 2015; Huguet et al., 1995; Minor et al., 2013; Mullor et al., 2001). Regulation of *Wnt* ligands by Shh is particularly relevant to the distinct expression pattern of *Wnt* ligands in the prostate. Mouse prostate stromal cells possess active Gli activity that is induced by the Shh ligands secreted by the basal cells (Peng et al., 2013). Interestingly, prostate basal cells are enriched in the proximal prostatic ducts. This may lead to an increased local Shh concentration and thereby an elevated Gli activity and Wnt ligand expression in the proximal prostatic stromal cells. Consistent with this theory, we found that when stromal cells isolated from the proximal prostatic ducts were cultured *in vitro*, the expression levels of *Wnt* ligands and *Axin2* were reduced dramatically (Figure S7C). This observation implies that the interaction between the basal cells and stromal cells regulates stromal expression of Wnt ligands, although it is also possible that the Wnt-expressing stromal cells were selected against during the *in vitro* culture. Second, Wnt ligands are also regulated by hormones such as the testosterone (Placencio et al., 2008; Tanaka et al., 2016). It has been well accepted that testosterone level within the prostate tissues is heterogeneous. Prostate stromal cells express the androgen receptor. Therefore, it is not impossible that the androgen differentially regulates expression of Wnt ligands in the stromal cells at distinct anatomic regions. Finally, cell shape and confluence are also shown to regulate Wnt ligand expression (Huguet et al., 1995). We noticed that the morphologies and densities of stromal cells in human TZ and PZ are different (X.W. and L.X., unpublished data). This may reflect the differences in extracellular matrix stiffness and composition between the two zones, which also actively regulate Wnt ligand expression.

We also discovered that Wnt/β-catenin signaling is differentially activated in both prostate epithelial cells and stromal cells at different anatomic locations. Although the proximal epithelial cells reside in a microenvironment that is rich in various Wnt ligands, they possess a lower canonical Wnt activity because of the antagonistic effect of Wnt5a as well as the relative lower expression of canonical Wnt receptors. Interestingly, a similar spatial regulation of the Wnt activity was also reported in the mammary gland epithelial ducts (Roarty et al., 2015), suggesting it represents a conserved mechanism for tissue patterning. On the other hand,

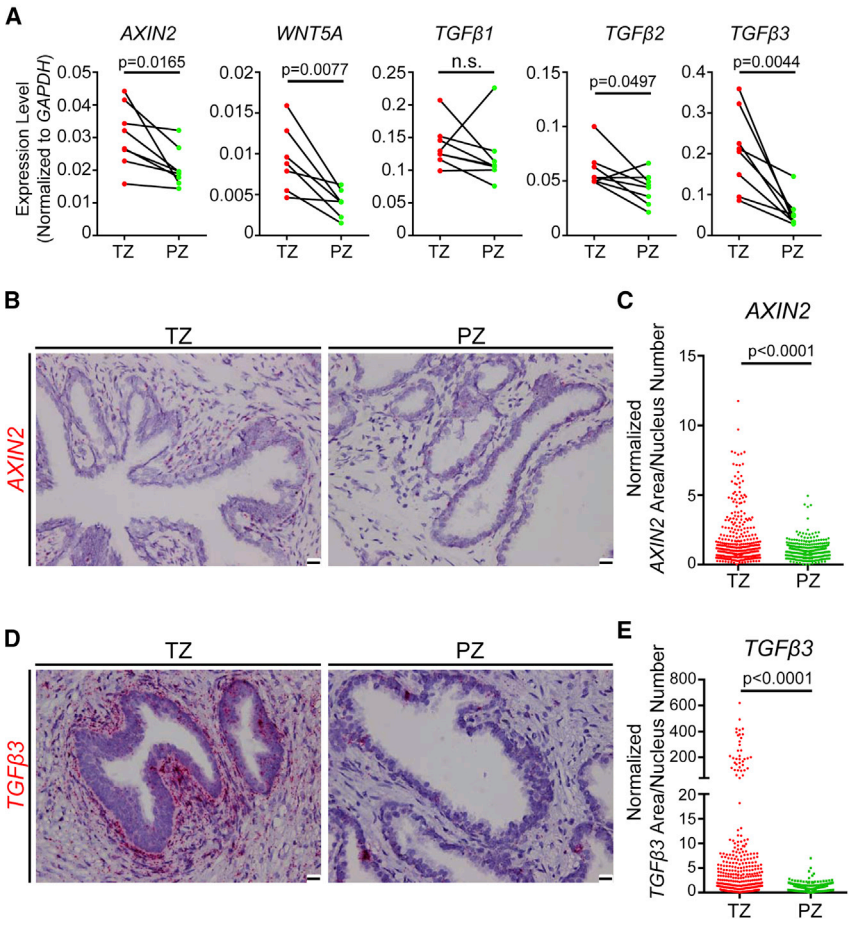

Figure 7. Wnt Signaling Is Higher in Stromal Cells of Human Transition Zone than in Peripheral Zone Prostate

(A) qRT-PCR analysis of *AXIN2*, *WNT5A*, *TGFB1*, *TGFB2*, and *TGFB3* in human TZ and PZ stromal cells obtained by laser capture microdissection. Data obtained from 7–8 pairs of formalin-fixed paraffin-embedded normal human TZ and PZ tissues. Statistical analysis performed by paired t test. TZ, transition zone; PZ, peripheral zone.

(B) RNA-*in situ* analysis of *AXIN2* in human TZ and PZ prostates. Scale bars, 20 μm.

(C) Dot graph shows quantification of *AXIN2* expression in human TZ and PZ. Data represent results from 9 independent human patient samples. Each dot represents result from one image. Staining areas of *AXIN2* in images of each pair of TZ and PZ are normalized by the average staining area in PZ of the same patient.

(D) RNA-*in situ* analysis of *TGFB3* in human TZ and PZ prostate. Scale bars, 20 μm.

(E) Dot graph shows quantification of *TGFB3* expression in human TZ and PZ. Data represent results from 9 independent human patient samples. Each dot represents result from one image. Staining areas of *TGFB3* in images of each pair of TZ and PZ are normalized by the average staining area in PZ of the same patient.

See also Figure S7.

Wnt/β-catenin signaling is preferentially activated in the proximal stromal cells because they express both more Wnt ligands and receptors. In addition, R-spondins, the Wnt signaling activators, are also expressed at a higher level in proximal prostatic stromal cells, although the difference is not statistically significant. These observations highlight that the status of the Wnt activity reflects combined input of various signaling components.

Benign prostatic hyperplasia (BPH) is a heterogeneous disease that results from nonmalignant proliferation of both the prostate epithelial and stromal compartment (Roehrborn, 2008). Pathological regeneration of stem cells in prostate epithelia and mesenchyme has been proposed as a cause for the tissue enlargement (Isaacs, 2008). Interestingly, BPH only occurs in the transition zone prostate. Our study shows that prostatic stromal Wnt signaling suppresses the epithelial proliferation directly and indirectly. Based on these facts, it is tempting to hypothesize that the stromal Wnt signaling is attenuated during BPH initiation and progression. Future studies using BPH specimens will test this hypothesis.

Wnt Signaling in Other Cell Lineages in Tissue Microenvironment

Besides the epithelial and stromal cells, other cell lineages such as the immune, endothelial, and nerve cells are also capable of responding to Wnt ligands, for example, Wnt signaling regulates T cell survival and lineage fate decisions (Gattinoni et al., 2010), dendritic cell-mediated immune tolerance (Swafford and Manicassamy, 2015), neurogenesis (Wang et al., 2012), and angiogenesis (Stenman et al., 2008). This implies that the differential expression pattern of Wnt ligands in distinct anatomic regions may result in different tissue microenvironment. Because of the complex and sometime contradictory roles of the Wnt signaling in different cell lineages, whether the overall tissue microenvironment is proinflammatory, immune-suppressive, or tumor-permissive will depend on the lineage composition in specific regions. It is tempting to hypothesize that such spatially restricted distinct tissue microenvironment determines region-specific prevalence or clinical behaviors of certain diseases, for example, why the frequency and aggressiveness of ductal versus alveolar adenocarcinoma are different in the same organ? This hypothesis is particularly interesting in the context of the prostate because the two major prostate-related diseases, prostate cancer and benign prostatic hyperplasia, occur preferentially in the peripheral and transition zones, respectively. It will be interesting to investigate whether the different gradient of stromal Wnt ligands in the two zones plays a role in the zonal specific prevalence of the two diseases.

STAR★METHODS

Detailed methods are provided in the online version of this paper and include the following:

- KEY RESOURCES TABLE
- CONTACT FOR REAGENT AND RESOURCE SHARING

SUPPLEMENTAL INFORMATION

Supplemental Information can be found online at https://doi.org/10.1016/j.stem.2019.03.010.

ACKNOWLEDGMENTS

We thank the Cytometry and Cell Sorting Core at Baylor College of Medicine (NIH AI036211, CA125123, and RR024574) for technical support and Joel M. Sederstrom for expert assistance. W.X. and B.D were supported by National Natural Science Foundation of China (81572536 and 81672850). This work was supported by NIDDK (R01DK092202 and R01DK107436 to L.X.).

AUTHOR CONTRIBUTIONS

Conceptualization, L.X. and X.W.; Investigation, X.W., L.Z., Z.Z., O.-J.K., R.D., and L.T.; Formal Analysis, X.W., L.X., L.Z., Z.Z., O.-J.K., Y.Z., and C.J.C.; Writing – Original Draft, L.X.; Writing – Review & Editing, L.X. with input from X.W. and C.J.C.; Resources, H.N., R.D., W.B., M.M.T., F.X., P.N., M.M.I., B.D., and W.X.; Funding Acquisition, L.X.; Supervision, L.X.

DECLARATION OF INTERESTS

The authors declare no competing interests.

Received: June 28, 2018
Revised: December 11, 2018
Accepted: March 10, 2019
Published: April 11, 2019

REFERENCES

Burger, P.E., Xiong, X., Coetzee, S., Salm, S.N., Moscatelli, D., Goto, K., and Wilson, E.L. (2005). Sca-1 expression identifies stem cells in the proximal region of prostatic ducts with high capacity to reconstitute prostatic tissue. Proc. Natl. Acad. Sci. USA *102*, 7180–7185.

Choi, N., Zhang, B., Zhang, L., Ittmann, M., and Xin, L. (2012). Adult murine prostate basal and luminal cells are self-sustained lineages that can both serve as targets for prostate cancer initiation. Cancer Cell *21*, 253–265.

Chua, C.W., Shibata, M., Lei, M., Toivanen, R., Barlow, L.J., Bergren, S.K., Badani, K.K., McKiernan, J.M., Benson, M.C., Hibshoosh, H., and Shen, M.M. (2014). Single luminal epithelial progenitors can generate prostate organoids in culture. Nature Cell Biol. *16*, 951–961.

Clevers, H., Loh, K.M., and Nusse, R. (2014). Stem cell signaling. An integral program for tissue renewal and regeneration: Wnt signaling and stem cell control. Science *346*, 1248012.

Collins, A.T., Habib, F.K., Maitland, N.J., and Neal, D.E. (2001). Identification and isolation of human prostate epithelial stem cells based on alpha(2) beta(1)-integrin expression. J. Cell Sci. *114*, 3865–3872.

Colombel, M., Vacherot, F., Diez, S.G., Fontaine, E., Buttyan, R., and Chopin, D. (1998). Zonal variation of apoptosis and proliferation in the normal prostate and in benign prostatic hyperplasia. Br. J. Urol. *82*, 380–385.

Creighton, C.J., Nagaraja, A.K., Hanash, S.M., Matzuk, M.M., and Gunaratne, P.H. (2008). A bioinformatics tool for linking gene expression profiling results with public databases of microRNA target predictions. RNA *14*, 2290–2296.

Ferrer-Vaquer, A., Piliszek, A., Tian, G., Aho, R.J., Dufort, D., and Hadjantonakis, A.K. (2010). A sensitive and bright single-cell resolution live imaging reporter of Wnt/ß-catenin signaling in the mouse. BMC Dev. Biol. *10*, 121.

Francis, J.C., Thomsen, M.K., Taketo, M.M., and Swain, A. (2013). β-catenin is required for prostate development and cooperates with Pten loss to drive invasive carcinoma. PLoS Genet. *9*, e1003180.

Gattinoni, L., Ji, Y., and Restifo, N.P. (2010). Wnt/beta-catenin signaling in T-cell immunity and cancer immunotherapy. Clin. Cancer Res. *16*, 4695–4701.

Goldstein, A.S., Huang, J., Guo, C., Garraway, I.P., and Witte, O.N. (2010). Identification of a cell of origin for human prostate cancer. Science *329*, 568–571.

Harada, N., Tamai, Y., Ishikawa, T., Sauer, B., Takaku, K., Oshima, M., and Taketo, M.M. (1999). Intestinal polyposis in mice with a dominant stable mutation of the beta-catenin gene. EMBO J. *18*, 5931–5942.

Hrycaj, S.M., Dye, B.R., Baker, N.C., Larsen, B.M., Burke, A.C., Spence, J.R., and Wellik, D.M. (2015). Hox5 Genes Regulate the Wnt2/2b-Bmp4-Signaling Axis during Lung Development. Cell Rep. *12*, 903–912.

Huang, L., Pu, Y., Hu, W.Y., Birch, L., Luccio-Camelo, D., Yamaguchi, T., and Prins, G.S. (2009). The role of Wnt5a in prostate gland development. Dev. Biol. *328*, 188–199.

Huelsken, J., Vogel, R., Erdmann, B., Cotsarelis, G., and Birchmeier, W. (2001). beta-Catenin controls hair follicle morphogenesis and stem cell differentiation in the skin. Cell *105*, 533–545.

Huguet, E.L., Smith, K., Bicknell, R., and Harris, A.L. (1995). Regulation of Wnt5a mRNA expression in human mammary epithelial cells by cell shape, confluence, and hepatocyte growth factor. J. Biol. Chem. *270*, 12851–12856.

Isaacs, J.T. (1985). Control of cell proliferation and death in normal and neoplastic prostate: A stem cell model. In Benigh prostatic hyperplasia, D.S. Coffey, C.H. Rodgers, and G.R. Cunha, eds. (NIH), pp. 85–94.

Isaacs, J.T. (2008). Prostate stem cells and benign prostatic hyperplasia. Prostate *68*, 1025–1034.

Karthaus, W.R., Iaquinta, P.J., Drost, J., Gracanin, A., van Boxtel, R., Wongvipat, J., Dowling, C.M., Gao, D., Begthel, H., Sachs, N., et al. (2014). Identification of multipotent luminal progenitor cells in human prostate organoid cultures. Cell *159*, 163–175.

Korinek, V., Barker, N., Moerer, P., van Donselaar, E., Huls, G., Peters, P.J., and Clevers, H. (1998). Depletion of epithelial stem-cell compartments in the small intestine of mice lacking Tcf-4. Nat. Genet. *19*, 379–383.

Kwon, O.J., Zhang, L., Ittmann, M.M., and Xin, L. (2014). Prostatic inflammation enhances basal-to-luminal differentiation and accelerates initiation of prostate cancer with a basal cell origin. Proc. Natl. Acad. Sci. USA *111*, E592–E600.

Kwon, O.J., Zhang, L., and Xin, L. (2016). Stem Cell Antigen-1 Identifies a Distinct Androgen-Independent Murine Prostatic Luminal Cell Lineage with Bipotent Potential. Stem Cell *34*, 191–202.

Lee, S.H., Johnson, D.T., Luong, R., Yu, E.J., Cunha, G.R., Nusse, R., and Sun, Z. (2015). Wnt/β-Catenin-Responsive Cells in Prostatic Development and Regeneration. Stem Cells *33*, 3356–3367.

Leong, K.G., Wang, B.E., Johnson, L., and Gao, W.Q. (2008). Generation of a prostate from a single adult stem cell. Nature *456*, 804–808.

Lescher, B., Haenig, B., and Kispert, A. (1998). sFRP-2 is a target of the Wnt-4 signaling pathway in the developing metanephric kidney. Dev. Dyn. *213*, 440–451.

Liu, J., Pascal, L.E., Isharwal, S., Metzger, D., Ramos Garcia, R., Pilch, J., Kasper, S., Williams, K., Basse, P.H., Nelson, J.B., et al. (2011). Regenerated luminal epithelial cells are derived from preexisting luminal epithelial cells in adult mouse prostate. Mol. Endocrinol. *25*, 1849–1857.

Lu, T.L., and Chen, C.M. (2015). Differential requirements for β-catenin in murine prostate cancer originating from basal versus luminal cells. J. Pathol. *236*, 290–301.

Lu, T.L., Huang, Y.F., You, L.R., Chao, N.C., Su, F.Y., Chang, J.L., and Chen, C.M. (2013). Conditionally ablated Pten in prostate basal cells promotes basal-to-luminal differentiation and causes invasive prostate cancer in mice. Am. J. Pathol. *182*, 975–991.

Madueke, I.C., Hu, W.Y., Huang, L., and Prins, G.S. (2018). WNT2 is necessary for normal prostate gland cyto-differentiation and modulates prostate growth in an FGF10 dependent manner. Am. J. Clin. Exp. Urol. *6*, 154–163.

Maeda, K., Kobayashi, Y., Udagawa, N., Uehara, S., Ishihara, A., Mizoguchi, T., Kikuchi, Y., Takada, I., Kato, S., Kani, S., et al. (2012). Wnt5a-Ror2 signaling between osteoblast-lineage cells and osteoclast precursors enhances osteoclastogenesis. Nat. Med. *18*, 405–412.

McNeal, J.E., Redwine, E.A., Freiha, F.S., and Stamey, T.A. (1988). Zonal distribution of prostatic adenocarcinoma. Correlation with histologic pattern and direction of spread. Am. J. Surg. Pathol. *12*, 897–906.

Miller, M.F., Cohen, E.D., Baggs, J.E., Lu, M.M., Hogenesch, J.B., and Morrisey, E.E. (2012). Wnt ligands signal in a cooperative manner to promote foregut organogenesis. Proc. Natl. Acad. Sci. USA *109*, 15348–15353.

Minor, P.J., He, T.F., Sohn, C.H., Asthagiri, A.R., and Sternberg, P.W. (2013). FGF signaling regulates Wnt ligand expression to control vulval cell lineage polarity in C. elegans. Development *140*, 3882–3891.

Mullor, J.L., Dahmane, N., Sun, T., and Ruiz i Altaba, A. (2001). Wnt signals are targets and mediators of Gli function. Curr. Biol. *11*, 769–773.

Nguyen, H., Merrill, B.J., Polak, L., Nikolova, M., Rendl, M., Shaver, T.M., Pasolli, H.A., and Fuchs, E. (2009). Tcf3 and Tcf4 are essential for long-term homeostasis of skin epithelia. Nat. Genet. *41*, 1068–1075.

Nusse, R., and Clevers, H. (2017). Wnt/β-Catenin Signaling, Disease, and Emerging Therapeutic Modalities. Cell *169*, 985–999.

Peng, Y.C., Levine, C.M., Zahid, S., Wilson, E.L., and Joyner, A.L. (2013). Sonic hedgehog signals to multiple prostate stromal stem cells that replenish distinct stromal subtypes during regeneration. Proc. Natl. Acad. Sci. USA *110*, 20611–20616.

Placencio, V.R., Sharif-Afshar, A.R., Li, X., Huang, H., Uwamariya, C., Neilson, E.G., Shen, M.M., Matusik, R.J., Hayward, S.W., and Bhowmick, N.A. (2008). Stromal transforming growth factor-beta signaling mediates prostatic response to androgen ablation by paracrine Wnt activity. Cancer Res. *68*, 4709–4718.

Reddy, S., Andl, T., Bagasra, A., Lu, M.M., Epstein, D.J., Morrisey, E.E., and Millar, S.E. (2001). Characterization of Wnt gene expression in developing and postnatal hair follicles and identification of Wnt5a as a target of Sonic hedgehog in hair follicle morphogenesis. Mech. Dev. *107*, 69–82.

Reya, T., Duncan, A.W., Ailles, L., Domen, J., Scherer, D.C., Willert, K., Hintz, L., Nusse, R., and Weissman, I.L. (2003). A role for Wnt signalling in self-renewal of haematopoietic stem cells. Nature *423*, 409–414.

Roarty, K., and Serra, R. (2007). Wnt5a is required for proper mammary gland development and TGF-beta-mediated inhibition of ductal growth. Development *134*, 3929–3939.

Roarty, K., Shore, A.N., Creighton, C.J., and Rosen, J.M. (2015). Ror2 regulates branching, differentiation, and actin-cytoskeletal dynamics within the mammary epithelium. J. Cell Biol. *208*, 351–366.

Roehrborn, C.G. (2008). Pathology of benign prostatic hyperplasia. Int. J. Impot. Res. *20* (*Suppl 3*), S11–S18.

Sato, A., Yamamoto, H., Sakane, H., Koyama, H., and Kikuchi, A. (2010). Wnt5a regulates distinct signalling pathways by binding to Frizzled2. EMBO J. *29*, 41–54.

Sato, T., van Es, J.H., Snippert, H.J., Stange, D.E., Vries, R.G., van den Born, M., Barker, N., Shroyer, N.F., van de Wetering, M., and Clevers, H. (2011). Paneth cells constitute the niche for Lgr5 stem cells in intestinal crypts. Nature *469*, 415–418.

Shahi, P., Seethammagari, M.R., Valdez, J.M., Xin, L., and Spencer, D.M. (2011). Wnt and Notch pathways have interrelated opposing roles on prostate progenitor cell proliferation and differentiation. Stem Cells *29*, 678–688.

Shoshkes-Carmel, M., Wang, Y.J., Wangensteen, K.J., Tóth, B., Kondo, A., Massasa, E.E., Itzkovitz, S., and Kaestner, K.H. (2018). Subepithelial telocytes are an important source of Wnts that supports intestinal crypts. Nature *557*, 242–246.

Silva, J., Barrandon, O., Nichols, J., Kawaguchi, J., Theunissen, T.W., and Smith, A. (2008). Promotion of reprogramming to ground state pluripotency by signal inhibition. PLoS Biol. *6*, e253.

Simons, B.W., Hurley, P.J., Huang, Z., Ross, A.E., Miller, R., Marchionni, L., Berman, D.M., and Schaeffer, E.M. (2012). Wnt signaling though beta-catenin is required for prostate lineage specification. Dev. Biol. *371*, 246–255.

Stenman, J.M., Rajagopal, J., Carroll, T.J., Ishibashi, M., McMahon, J., and McMahon, A.P. (2008). Canonical Wnt signaling regulates organ-specific assembly and differentiation of CNS vasculature. Science *322*, 1247–1250.

Swafford, D., and Manicassamy, S. (2015). Wnt signaling in dendritic cells: its role in regulation of immunity and tolerance. Discov. Med. *19*, 303–310.

Tanaka, T., Kanatsu-Shinohara, M., Lei, Z., Rao, C.V., and Shinohara, T. (2016). The Luteinizing Hormone-Testosterone Pathway Regulates Mouse Spermatogonial Stem Cell Self-Renewal by Suppressing WNT5A Expression in Sertoli Cells. Stem Cell Reports *7*, 279–291.

Tsujimura, A., Koikawa, Y., Salm, S., Takao, T., Coetzee, S., Moscatelli, D., Shapiro, E., Lepor, H., Sun, T.T., and Wilson, E.L. (2002). Proximal location of mouse prostate epithelial stem cells: a model of prostatic homeostasis. J. Cell Biol. *157*, 1257–1265.

Valdez, J.M., Zhang, L., Su, Q., Dakhova, O., Zhang, Y., Shahi, P., Spencer, D.M., Creighton, C.J., Ittmann, M.M., and Xin, L. (2012). Notch and TGFβ form a reciprocal positive regulatory loop that suppresses murine prostate basal stem/progenitor cell activity. Cell Stem Cell *11*, 676–688.

van Amerongen, R., Bowman, A.N., and Nusse, R. (2012). Developmental stage and time dictate the fate of Wnt/β-catenin-responsive stem cells in the mammary gland. Cell Stem Cell *11*, 387–400.

Wang, X., Kopinke, D., Lin, J., McPherson, A.D., Duncan, R.N., Otsuna, H., Moro, E., Hoshijima, K., Grunwald, D.J., Argenton, F., et al. (2012). Wnt signaling regulates postembryonic hypothalamic progenitor differentiation. Dev. Cell *23*, 624–636.

Wang, Z.A., Mitrofanova, A., Bergren, S.K., Abate-Shen, C., Cardiff, R.D., Califano, A., and Shen, M.M. (2013). Lineage analysis of basal epithelial cells reveals their unexpected plasticity and supports a cell-of-origin model for prostate cancer heterogeneity. Nat. Cell Biol. *15*, 274–283.

Xin, L., Ide, H., Kim, Y., Dubey, P., and Witte, O.N. (2003). In vivo regeneration of murine prostate from dissociated cell populations of postnatal epithelia and urogenital sinus mesenchyme. Proc. Natl. Acad. Sci. USA *100* (*Suppl 1*), 11896–11903.

Xin, L., Lawson, D.A., and Witte, O.N. (2005). The Sca-1 cell surface marker enriches for a prostate-regenerating cell subpopulation that can initiate prostate tumorigenesis. Proc. Natl. Acad. Sci. USA *102*, 6942–6947.

Xin, L., Lukacs, R.U., Lawson, D.A., Cheng, D., and Witte, O.N. (2007). Self-renewal and multilineage differentiation in vitro from murine prostate stem cells. Stem Cells *25*, 2760–2769.

Yamane, T., Kunisada, T., Tsukamoto, H., Yamazaki, H., Niwa, H., Takada, S., and Hayashi, S.I. (2001). Wnt signaling regulates hemopoiesis through stromal cells. J. Immunol. *167*, 765–772.

Yochum, G.S., Cleland, R., and Goodman, R.H. (2008). A genome-wide screen for beta-catenin binding sites identifies a downstream enhancer element that controls c-Myc gene expression. Mol. Cell. Biol. *28*, 7368–7379.

Yoo, Y.A., Roh, M., Naseem, A.F., Lysy, B., Desouki, M.M., Unno, K., and Abdulkadir, S.A. (2016). Bmi1 marks distinct castration-resistant luminal progenitor cells competent for prostate regeneration and tumour initiation. Nat. Commun. *7*, 12943.

Yu, X., Wang, Y., DeGraff, D.J., Wills, M.L., and Matusik, R.J. (2011). Wnt/β-catenin activation promotes prostate tumor progression in a mouse model. Oncogene *30*, 1868–1879.

Zhang, B., Kwon, O.J., Henry, G., Malewska, A., Wei, X., Zhang, L., Brinkley, W., Zhang, Y., Castro, P.D., Titus, M., et al. (2016). Non-Cell-Autonomous Regulation of Prostate Epithelial Homeostasis by Androgen Receptor. Mol. Cell *63*, 976–989.

Zhang, D., Jeter, C., Gong, S., Tracz, A., Lu, Y., Shen, J., and Tang, D.G. (2018). Histone 2B-GFP Label-Retaining Prostate Luminal Cells Possess Progenitor Cell Properties and Are Intrinsically Resistant to Castration. Stem Cell Reports *10*, 228–242.

Zhao, C., Cai, S., Shin, K., Lim, A., Kalisky, T., Lu, W.J., Clarke, M.F., and Beachy, P.A. (2017). Stromal *Gli2* activity coordinates a niche signaling program for mammary epithelial stem cells. Science *356*, eaal3485.

Zheng, D., Decker, K.F., Zhou, T., Chen, J., Qi, Z., Jacobs, K., Weilbaecher, K.N., Corey, E., Long, F., and Jia, L. (2013). Role of WNT7B-induced noncanonical pathway in advanced prostate cancer. Mol. Cancer Res. *11*, 482–493.

STAR★METHODS

KEY RESOURCES TABLE

REAGENT or RESOURCE	SOURCE	IDENTIFIER
Antibodies		
Rat anti-Mouse CD31-eFluor 450 (Clone 390)	eBioscience	Cat# 48-0311-82; RRID:AB_10598807
Rat anti-Mouse CD45-eFluor 450 (Clone 30-F11)	eBioscience	Cat# 48-0451-82; RRID:AB_1518806
Rat anti-Mouse Ter119-eFluor 450 (Clone TER-119)	eBioscience	Cat# 48-5921-82; RRID:AB_1518808
Rat anti-Mouse CD49f-APC (Clone eBioGoH3)	eBioscience	Cat# 17-0495-82; RRID:AB_2016694
Rat anti-Mouse Sca1-PE (Clone D7)	eBioscience	Cat# 12-5981-83; RRID:AB_466087
Rat anti-Mouse CD24-PECy7 (Clone M1/69)	BD Biosciences	Cat# 560536; RRID:AB_1727452
Mouse anti-BrdU-FITC (Clone BU20A)	eBioscience	Cat# 11-5071-42; RRID:AB_11042627
Rabbit anti-Mouse K5 (Clone Poly19055)	Covance	Cat# PRB-160P; RRID:AB_2565050
Mouse anti-Mouse K8 (Clone 1E8)	Covance	Cat# MMS-162P; RRID:AB_2565043
Mouse anti-Mouse K14 (Clone LL002)	Santa Cruz Biotechnology	Cat# sc-58724; RRID:AB_784170
Mouse anti-Mouse P63 (Clone 4A4)	Abcam	Cat# ab735; RRID:AB_305870
Chicken anti-GFP	Abcam	Cat# ab13970; RRID:AB_300798
Rat anti-BrdU (Clone BU1/75)	Abcam	Cat# ab6326; RRID:AB_305426
Rabbit anti-Mouse Ki67	Leica Biosystems	Cat# NCL-Ki67-P; RRID:AB_442102
Rabbit anti-Mouse AR	Santa Cruz Biotechnology	Cat# sc-816; RRID:AB_1563391
Rabbit anti-Mouse Cleaved Caspase 3	Cell Signaling Technology	Cat# 9661S; RRID:AB_2341188
Rat anti-Mouse Sca-1 (Clone D7)	BD Pharmingen	Cat# 557403; RRID:AB_396686
Mouse anti-Mouse Smooth Muscle Actin (Clone 1A4)	Sigma-Aldrich	Cat# 202M; RRID:AB_1157937
Rabbit anti-Mouse Vimentin	Cell Signaling Technology	Cat# 5741S; RRID:AB_10695459
Mouse anti-Mouse E-cadherin (Clone 36/E-Cadherin)	BD Transduction Labs	Cat# 610181; RRID:AB_397580
Rabbit anti-Mouse Nkx3.1	Athena Enzyme Systems	Cat# 0315
Mouse anti-Mouse Ror2	Developmental studies hybridoma bank	Cat# Nt 2535-2835; RRID:AB_10804796
Rabbit anti-Mouse CD31	Abcam	Cat# ab28364; RRID:AB_726362
Rat anti-Mouse CD45 (Clone 30-F11)	BD Pharmingen	Cat# 550539; RRID:AB_2174426
Rabbit anti-Mouse pSmad3 (pS423/pS425)	Rockland	Cat# 600-401-919; RRID:AB_2192878
Rabbit anti-Mouse Smad2/3	Cell Signaling Technology	Cat# 5678; RRID:AB_10693547
Mouse anti-Mouse β-actin (Clone AC-74)	Sigma-Aldrich	Cat# A2228; RRID:AB_476697
Goat α-Mouse IgG(H+L) Alexa Fluor 488	Invitrogen	Cat# A11017; RRID:AB_2534084
Goat α-Mouse IgG(H+L) Alexa Fluor 594	Invitrogen	Cat# A11020; RRID:AB_2534087
Goat α-Rabbit IgG(H+L) Alexa Fluor 488	Invitrogen	Cat# A11034; RRID:AB_2576217
Goat α-Rabbit IgG(H+L) Alexa Fluor 594	Invitrogen	Cat# A11037; RRID:AB_2534095
Goat α-Rat IgG(H+L) Alexa Fluor 488	Invitrogen	Cat# A11006; RRID:AB_2534074
Goat α-Rat IgG(H+L) Alexa Fluor 594	Invitrogen	Cat# A11007; RRID:AB_10561522
Horse α-Mouse IgG(H+L) HRP	Vector Lab.	Cat# PI-2000; RRID:AB_2336177
Goat α-Rabbit IgG(H+L) HRP	Vector Lab.	Cat# PI-1000; RRID:AB_2336198
Biological Samples		
Human PZ and TZ prostate specimens	Michael E. DeBakey Veteran Medical Center, U.S.	N/A
Chemicals, Peptides, and Recombinant Proteins		
Tamoxifen	Sigma-Aldrich	Cat# T5648
BrdU	Sigma-Aldrich	Cat# B5002-5G

(*Continued on next page*)

Continued

REAGENT or RESOURCE	SOURCE	IDENTIFIER
Wnt3a	R&D	Cat#1324-WN-002
Wnt5a	R&D	Cat# 645-WN-010
Tgfβ1	R&D	Cat# 240-B-002
Tgfβ2	R&D	Cat# 302-B2-002
Tgfβ3	R&D	Cat# 8420-B3-005
Critical Commercial Assays		
NucleoSpin RNA Kit	Macherey-Nagel	Cat# 740955
NucleoSpin RNA XS Kit	Macherey-Nagel	Cat# 740902
SsoAdvanced PreAmp Supermix	Bio-rad	Cat# 172-5160
WNT Signaling Pathway RT^2 Profiler PCR Array	QIAGEN	Cat# 330231 PAMM-043Z
RT^2 First Strand Kit	QIAGEN	Cat# 330401
RT^2 PreAMP Wnt Pathway Primer Mix	QIAGEN	Cat# PBM-043Z
RT^2 PreAMP cDNA Synthesis Kit	QIAGEN	Cat# 330451
RT^2 SYBR Green ROX qPCR Mastermix	QIAGEN	Cat# 330522
BD Pharmingen BrdU Flow Kit	BD	Cat# 559619
SMART-Seq v4 Ultra Low Input RNA Kit	Clontech	Cat# 634888
Nextera XT DNA Library Preparation Kit	Illumina	Cat# FC-131-1024
TruSeq Stranded mRNA Library Prep Kit	Illumina	Cat# 20020594
Q5 Site-Directed Mutagenesis Kit	New England Lab	Cat# E0554S
RNA-Scope 2.5 HD Detection Reagent Red Kit	Advanced Cell Diagnostics	Cat# 322360
truXTRAC FFPE RNA microTUBE Kit	Covaris	Cat# 520161
MasterPure RNA Purification Kit	Illumina	Cat# MCR85102
Deposited Data		
RNA-seq data of the stromal cells at proximal and distal prostatic ducts	This paper	GEO: GSE115631
RNA-seq data of the basal cells at proximal and distal prostatic ducts	This paper	GEO: GSE72318
RNA-seq data of the prostate stromal cells expressing S37A β-Catenin and RFP	This paper	GEO: GSE115467
Experimental Models: Organisms/Strains		
Mouse: C57BL/6	Charles River	Strain code: 027
Mouse: SCID/Beige	Charles River	Strain code: 250
Mouse: Col1a2-$CreER^{T2}$	Jackson Laboratory	JAX stock #029567
Mouse: B6.Cg-*Gt(ROSA)26Sor*$^{tm3(CAG-EYFP)Hze}$/J	Jackson Laboratory	JAX stock #007903
Mouse: *TCF/Lef:*H_2B*-GFP*	Jackson Laboratory	JAX stock #013752
Mouse: Ctnnb1$^{loxp/loxp}$	Baylor College of Medicine, U.S.	Kind Gift from Hoang Nugyen
Mouse: Ctnnb1$^{lox(ex3)}$	Baylor College of Medicine, U.S.	Kind Gift from Hoang Nugyen
Oligonucleotides		
Primers for genotyping of mouse lines, see Table S2	This paper	N/A
qPCR Primers for human genes, see Table S2	This paper	N/A
qPCR Primers for mouse genes, see Table S2	This paper	N/A
qPCR Primers for ChIP assay, see Table S2	This paper	N/A
Primers for *Tgfβ 2/3* Luciferase Reporter Cloning, see Table S2	This paper	N/A
Recombinant DNA		
Plasmid: FU-CGW	Xin et al., 2003	N/A
Plasmid: FU-CRW	Xin et al., 2003	N/A
cDNA: S37A *β-Catenin*	UCLA, U.S.	Kind Gift from Roger Lo

(*Continued on next page*)

Continued

REAGENT or RESOURCE	SOURCE	IDENTIFIER
cDNA: dominant-negative β-Catenin	MD Anderson Cancer Center, U.S.	Kind Gift from Pierre Mccrea
cDNA: dominant-negative TgfβRII	NIH, U.S.	Kind Gift from Lalage Wakefield
Software and Algorithms		
Leica Application Suite X	Leica Microsystems GmbH	RRID:SCR_013673; URL: https://www.leica-microsystems.com/products/microscope-software/details/product/leica-las-x-ls/
FlowJo	Tree Star	RRID:SCR_008520; URL:https://www.flowjo.com/solutions/flowjo
GraphPad Prism 7	GraphPad Software	RRID:SCR_002798
Image-Pro Plus version 6.3	Media Cybernetics	RRID:SCR_007369
Fiji	ImageJ	RRID: SCR_002285
Adobe Photoshop CC	Adobe Systems	RRID: SCR_014199
Adobe Illustrator CC	Adobe Systems	RRID: SCR_010279
Other		
FISH probe: human *AXIN2*	Advanced Cell Diagnostics	N/A
FISH probe: human *TGFβ3*	Advanced Cell Diagnostics	N/A

CONTACT FOR REAGENT AND RESOURCE SHARING

Further information and requests for resources and reagents should be directed to and will be fulfilled by the Lead Contact, Li Xin (xin18@uw.edu)

EXPERIMENTAL MODEL AND SUBJECT DETAILS

Mice

All animals used in this study received humane care in compliance with the principles stated in the Guide for the Care and Use of Laboratory Animals, NIH Publication, 1996 edition, and the protocol was approved by the Institutional Animal Care Committee of Baylor College of Medicine and University of Washington. The C57BL/6 and SCID/Beige mice were purchased from Charles River (Wilmington, MA). Col1a2-CreER^{T2}, and B6.Cg-*Gt(ROSA)26Sor*$^{tm3(CAG-EYFP)Hze}$/J mice were purchased from the Jackson Laboratory (Bar Harbor, ME). TCF/LEF:H_2B-GFP reporter line, Ctnnb1$^{loxp/loxp}$, and Ctnnb1$^{lox(ex3)}$ were described previously (Ferrer-Vaquer et al., 2010; Harada et al., 1999; Huelsken et al., 2001) and were obtained from Dr. Hoang Nugyen at the Baylor College of Medicine. Mice were genotyped by polymerase chain reaction using mouse genomic DNA from tail biopsy specimens. The sequences of genotyping primers and the expected band sizes for PCR are listed in Table S2. PCR products were separated electophoretically on 1% agarose gels and visualized via ethidium bromide under UV light.

Human specimens

Human PZ and TZ prostate specimens used in this study were obtained from patients undergoing open simple prostatectomy for prostate cancer at the Michael E. DeBakey Veteran Medical Center with Institutional Review Board approval. Peripheral zone tissues were obtained from patients with relatively smaller localized tumors (prostate weights between 25-35 g), and tissues were collected distant from major tumor nodules. Fresh specimens were fixed in 10% buffered formalin for 24 hours and processed for RNA-*In Situ* analyses. Specimens were confirmed to be cancer free by histological and immunostaining of CK5 and P63.

METHOD DETAILS

Tamoxifen and BrdU treatment

Tamoxifen (Sigma-Aldrich, St. Louis, MO) was dissolved in corn oil and administrated i.p. into experimental mice at the specified age (5 mg/40 g/day for four consecutive days unless otherwise specified). BrdU (Sigma-Aldrich, St. Louis, MO) (80mg/kg/day) was administrated 3 days before mice were sacrificed unless otherwise specified.

Cell culture

8∼12-week-old C57BL/6 mouse prostate tissues were digested and dissociated into single cells as described previously (Zhang et al., 2016). Dissociated single cells were cultured in Biocoat^{TM} Collage I-coated plates (Corning, Corning, NY) in Bfs medium (5% Nu-Serum, 5% FBS, 1 × Insulin/Selenium, 1 × L-Glutamine, 1 × Penicillin/Streptomycin, and 1 × 10^{-10}M DHT in DMEM

medium) at 37°C with 5% CO_2. When the cell confluency reached around 90%, cells were trypsinized into single cells with 0.25% Trypsin-EDTA (Invitrogen, Carlsbad, CA). Cells were replated in Biocoat™ Collage I-coated plates (Corning, Corning, NY) for 30 min at 37°C/5% CO_2. Unattached cells were discarded, and remaining cells were cultured in Bfs at 37°C/5% CO_2 till 80%–90% confluency. All the experiments in this study used fresh primary stromal cells within 3 weeks after single cell dissociation from prostates.

Flow cytometry and cell sorting

Dissociated single mouse prostate cells were incubated with florescence conjugated antibodies at 4°C for 30 minutes. Information for antibodies for FACS analysis and sorting is listed in the Key Resources Table. FACS analyses and sorting were performed by using the BD LSR II, BD LSR Fortessa, Aria I (BD Biosciences, San Jose, CA).

RNA isolation, quantitative RT–PCR, and RT^2 Profiler™ PCR array

Total RNA was extracted using Nucleospin RNA extraction Kit (Macherey-Nagel, Bethlehem, PA). RNA was reverse transcribed to cDNA using iScript™ Reverse Transcriptase Kit (BioRad, Hercules, CA). QRT-PCR was performed using iTaq™ Universal SYBR Green Supermix (BioRad, Hercules, CA) and detected on a StepOne plus Real-Time PCR system (Applied Biosystems, Foster City, CA). Primers for target genes were listed in Table S2. Analysis of the Wnt signaling components was performed on RT^2 Profiler™ PCR Array Mouse Wnt signaling plates following the manufacturer's instruction (QIAGEN, Valencia, CA).

qRT-PCR from Laser captured FFPE tissues

Slides of 10 μm were sectioned from FFPE blocks using a Leica RM 2253 microtome, mounted onto Arcturus PEN Membrane Frame Slides (Thermo Scientific, Waltham, MA), and dried overnight at room temperature. Sections were stained with Cresyl Violet (Acros Organic, New Jersey, NJ) and left at room temperature for one hour to dry. Adjacent sections of 5 μm were cut and stained with hematoxylin and eosin. Histology review and slide annotation was performed by pathologist. Areas of cancer, PIN, and extensive inflammation were marked if present and were excluded from the subsequent experiments. Areas of stroma within 120 microns of a benign gland or 240 microns between benign glands were captured using the Arcturus XT (Thermo Scientific, Waltham, MA) with CapSure Macro LCM Caps (Thermo Scientific, LCM0211) and RNA was extracted using the truXTRAC FFPE RNA microTUBE Kit (Covaris, Woburn, MA) according to manufacturer's recommendations. RNA quality (DV200) and quantity were assessed using the TapeStation 4200 (Agilent Technologies, Santa Clara, CA) with High Sensitivity RNA Screentape (Agilent Technologies, Santa Clara, CA). RNA was reverse transcribed to cDNA using iScript Reverse Transcriptase kit (BioRad, Hercules, CA). cDNA was pream-plified using SsoAdvanced PreAmp Supermix (BioRad, Hercules, CA). QRT-PCR was performed using iTaq™ Universal SYBR Green Supermix (BioRad, Hercules, CA) and detected on a Quantstudio Real-Time PCR system (Applied Biosystems, Foster City, CA).

Lentivirus preparation

CDNAs for S37A *β-Catenin*, dominant negative *β-Catenin*, and dominant negative *TgfβRII* were gifts from Dr. Roger Lo at UCLA, Dr. Pierre Mccrea at MD Anderson Cancer Center, and Dr. Lalage Wakefield at NIH, respectively. cDNA was cloned into the FU-CGW or FU-CRW lentiviral vector (Xin et al., 2003) at the EcoRI site. Lentivirus preparation, titering, and infection of UGSM cells or dissociated prostate cells were performed as described previously (Xin et al., 2003).

Prostate sphere assay

The prostate sphere assay was performed as described previously (Xin et al., 2007). Briefly, 1 × 10^4 dissociated prostate cells were mixed in 1:1 Matrigel/PrEGM (Matrigel (BD Biosciences, San Jose, CA)/PrEGM (Lonza, Walkersville, MD)), plated in 12-well plates, and cultured in PrEGM medium. Prostate spheres were defined as spheroids with a diameter > 30 μm after a 6-day culture. When prostate basal cells were cocultured with stromal cells or urogenital sinus mesenchymal cells, the ratio of epithelial versus stromal cells is 1:2.

Prostate organoid culture

The organoid culture was performed as described previously (Karthaus et al., 2014). Briefly, dissociated prostate cells from 8-12 week-old C57BL/6 mice were cultured in DMEM/F12 supplemented with B27 (Life technologies, Grand Island, NY), 10 mM HEPES, Glutamax (Life technologies, Grand Island, NY), Penicillin/Streptomycin, and the following growth factors: EGF 50 ng/ml (Peprotech, Rocky Hill, NJ), 500 ng/ml recombinant R-spondin1 (Peprotech, Rocky Hill, NJ), 100 ng/ml recombinant Noggin (Peprotech, Rocky Hill, NJ), 200 μM TGF-β/Alk inhibitor A83-01 (Tocris, Ellisville, MO), and 10 μM Y-27632 (Tocris, Ellisville, MO). Dihydrotestosterone (Sigma, St. Louis, MO) was added at 1 nM final concentration. Cells were resuspended in growth factor reduced matrigel (Corning, Corning, NY) and plated in 96-well plates.

Prostate regeneration assay

8-12 week old mouse prostate tissues were dissociated into single cells by the procedure described previously (Kwon et al., 2016; Valdez et al., 2012). UGSM cell preparation and prostate regeneration assays were performed as described previously (Xin et al.,

2003). Briefly, 1x10^5 wild-type or lentivirus-infected dissociated prostate cells were mixed with 1x10^5 wild-type or lentivirus-infected murine UGSM cells in type I collagen extracted from rat tails. Cell mixtures were grafted under the renal capsules of immunodeficient male SCID/Bg mice and incubated for 8 weeks.

RNA-seq

NucleoSpin RNA XS Kit (Macherey-Nagel, Bethlehem, PA) was used to purify RNAs from FACS-isolated proximal and distal mouse prostate basal and stromal cells. Reverse transcriptions were performed using SMART Seq^{TM} v4 Ultra^{TM} Low Input RNA Kit for Sequencing (Clontech Laboratories, Mountain View, CA). CDNA libraries were prepared using Nextera XT DNA Library Preparation Kit (Illumina, San Diego, CA).

RNA was extracted from the β-Catenin S37A-expressing mouse prostate stromal cells and RFP-expressing control stromal cells using MasterPure^{TM} RNA Purification Kit (Illumina, San Diego, CA). TruSeq Stranded mRNA Sample Preparation Kit (Illumina, San Diego, CA) was used to prepare cDNA libraries, which were sequenced using HiSeq 2500 sequencer. Sequenced reads in FASTQ files were mapped to mm10 whole genome using Tophat2, and Fragments Per Kilobase of transcript per Million mapped reads (FPKM) were calculated using Cufflinks. Genes found differentially expressed ($p < 0.05$ by t test, and minimum fold change of 1.4 or 1.2) were evaluated for enrichment of Gene Ontology (GO) gene classes, using SigTerms software (Creighton et al., 2008). Data have been deposited at GEO.

ChIP assay

Briefly, primary mouse prostate stromal cells were crosslinked in cell culture media containing 1% methanol free formaldehyde (Polysciences, Warrington, PA) for 10 minutes at room temperature. Cross-linking was terminated by adding 125 mM Glycine for 5 minutes at room temperature. Cells were harvested in PBS containing protease inhibitors and PMSF. Subsequently, cells were re-suspended in sonication buffer and sonicated. Input samples were taken following sonication. The remaining sonication product was divided into 2 halves incubated with 4μg antibodies against β-Catenin (610154, BD Biosciences, San Jose, CA) or normal rabbit IgG (sc-2027, Santa Cruz Biotech, Santa Cruz, CA) in ChIP Buffer 1 containing protease inhibitors and magnetic G beads overnight at 4°C *in silico*nized tubes. Beads were collected and washed with ChIP Buffer 1 and ChIP Buffer 2. Beads were then resuspended in elution buffer for 15 minutes at room temperature. Formaldehyde crosslinks were reversed by incubating samples in reverse cross-linking buffer at 65°C for 2.5 hours. Remaining proteins were digested with Proteinase K (50μg/μl) at 37°C for 1 hour. DNA was then isolated using the Purelink Quick Gel Extraction Kit (Invitrogen, Carlsbad, CA). qRT-PCR was performed to determine enrichment using the primers listed in Table S2. Ct values from α-IgG and α-β-Catenin were normalized against Ct values generated from the input samples. The resulting value was then normalized by dilution and concentration to determine the value relative to the input.

Luciferase reporter assay

A 2 and 4 Kb genomic sequence upstream of the translational start codon of the mouse Tgfβ2 and 3, respectively, containing multiple TCF/LEFs binding sites confirmed by the ChIP analysis was PCR amplified from two BAC clones from the BACPAC Resources Center (Children's Hospital Oakland Research Institute) containing the corresponding genomic region using LA Taq (Takara Bio Inc., Otsu, Shiga, Japan). The primers used are listed in Table S2. The amplicon was cloned into the pGL3 luciferase vector (Promega, Madison, WI) via the KpnI and BglII restriction sites upstream of luciferase generating the pGL3-Tgfβ2-luc and pGL3-Tgfβ3-luc reporters. Mutations in the TCF/LEFs binding sites were performed by site-directed-mutagenesis using the Q5® Site-Directed Mutagenesis kit (New England Lab, Woburn, MA).

Primary mouse prostate stromal cells were infected with either FU-CRW or FU-β-catenin S37A-CRW. Two days later, cells were seeded in 6 well plates and co-transfected with 40 ng of pRL-CMV Renilla and 2ug of pGL3-Tgfβ2-luc, pGL3-Tgfβ3-luc, or corresponding mutant constructs, respectively, using lipofectamine 3000 according to the manufacturer's instructions. Two days after transfection, the Bfs cell culture medium was replaced with 1:10 Opti-MED diluted Bfs medium. 24 hours later, luciferase activity was measured using the dual-Luciferase reporter assay system (Promega, Madison, WI). Firefly luciferase activity was normalized to CMV-Renilla luciferase activity.

RNA-Scope

TZ and PZ tissues collected from the same donors were collected at the same time and fixed by 10% neutral buffered formalin for 16∼32 hours at room temperature. Samples were embedded in paraffin blocks and cut into 5um sections for staining. Freshly cut slides were air-dried overnight at room temperature, then baked for 1 hour at 60°C. The RNA-Scope *in situ* hybridization was performed by using RNA-Scope 2.5 HD Detection Reagent Red Kit (Advanced Cell Diagnostics, Newark, CA) following the manufacturer's standard protocol. 20-60 images were taken for each sample to cover all areas of the stained specimens. For analysis, we focused on the stromal cells adjacent to the epithelial compartment. We used the Image-Pro Plus version 6.3 by Media Cybernetics to include all inter-glandular areas that were within a range of 150 um away from the basement membrane between the epithelial and stromal compartments. Nuclei numbers and areas with staining of *AXIN2* and *TGFβ3* in the defined areas were determined by the count feature in the software. Total *AXIN2* or *TGFβ3* staining areas within the stromal cells were normalized by nucleus number of stromal cells on each image. Images of each pair of TZ and PZ samples were further normalized by the average value of the PZ staining area of the same patient so that data from different patients can be pooled for analysis shown in Figure 7.

Western blots

Cells were lysed in RIPA buffer (20 mM Tris-HCl, pH 7.5, 150 mM NaCl, 1 mM Na_2EDTA, 1 mM EGTA, 1% NP-40, 1% sodium deoxycholate, 2.5 mM sodium pyrophosphate, 1 mM β-glycerophosphate, 1 mM Na_3VO_4) with protease inhibitors and phosphatase inhibitors (Roche Applied Science, Indianapolis, IN). Protein concentrations were determined by a Bradford Assay kit (BioRad, Hercules, CA). Protein was separated by 10% SDS/PAGE and transferred onto a nitrocellulose membrane (Amersham Biosciences, Arlington Heights, IL). The membrane was blocked in 5% skim milk, and subsequently incubated with primary antibodies listed in the Key Resources Table at 4°C overnight followed by incubation with peroxidase-conjugated goat anti-mouse IgG or goat anti-rabbit IgG (Jackson ImmunoResearch, Inc., West Grove, PA), and developed with Pierce ECL reagent (Thermal Scientific, Rockford, IL).

Histology and Immunostaining

Prostate tissues were fixed by 10% buffered formalin and paraffin embedded. HE staining and immunofluorescence staining were performed with 5 μm sections. For hematoxylin and eosin staining, sections were processed as described previously (Choi et al., 2012). For immunostaining, sections were processed as described previously (Choi et al., 2012) and incubated with primary antibody in 3% of normal goat serum (Vector Laboratories, Burlingame, CA) overnight. Information for primary antibodies is listed in the Key Resources Table. Slides then were incubated with secondary antibodies (diluted 1:250 in PBST) labeled with Alexa Fluor 488 and 594 (Invitrogen/Molecular Probes, Eugene, OR). Sections were counterstained with 4,6-diamidino-2-phenylindole (DAPI) (Sigma-Aldrich, St. Louis, MO). Immunofluorescence staining was imaged using an Olympus BX60 fluorescence microscope (Olympus Optical Co Ltd, Tokyo, Japan) or a Leica EL6000 confocal microscope (Leica Microsystems, Wetzlar, Germany). Images of IHC were analyzed by Image-Pro Plus version 6.3 by Media Cybernetics. Cell number was determined by using the count feature in the software which asks for the user to indicate the color that would be used to indicate a positive cell (For example: blue would be indicated to count nuclei and thus indicate total numbers of cells).

QUANTIFICATION AND STATISTICAL ANALYSIS

All experiments were performed using 3-10 mice in independent experiments. Data are presented as mean ± s.d. Student's t test and one-way ANOVA with multiple comparisons were used to determine significance in two-group and multiple-group experiments, respectively. For all statistical tests, the two-tail $p \leq 0.05$ level of confidence was accepted for statistical significance. More details are found in the figure legends.

DATA AND SOFTWARE AVAILABILITY

The accession numbers for the RNA-seq data of the stromal cells at proximal and distal prostatic ducts, basal cells at proximal and distal prostatic ducts, stromal cells expressing S37A β-Catenin and RFP in this paper are GEO: GSE115631, GEO: GSE72318, GEO: GSE115467, respectively. Detailed descriptions of data analysis and the software used can be found in METHOD DETAILS.